

The discovery of igneous xenoliths in the Upper Zone of
the Bushveld Igneous Complex and its implications on the
model of emplacement of Upper Zone magmas.

Submitted as partial requirement for the degree

MSc Geology

Submitted to:

Department of Geology

School of Physical Sciences

Faculty of Natural and Agricultural Sciences

University of Pretoria

Submitted by:

Adriana Alberts

15182322

Date of Final Version:

31/10/2023

DECLARATION:

I, the undersigned, declare that the thesis/ dissertation, which I hereby submit for the degree MSc Geology at the University of Pretoria, is my own work and has not previously been submitted by me for a degree at this or any other tertiary institution.

Full names: Adriana Christina Alberts

Student number: 15182322

Date submitted: 31/10/2023

Degree: MSc Geology

Topic of work: Investigating the origin of geological anomalies believed to be xenoliths in the Upper Zone of the Bushveld Igneous Complex in the Roossenekal area.

Supervisor: Dr James Roberts, Department of Geology

ACKNOWLEDGEMENTS

I would like to express my sincere gratitude to Prof. James Roberts, my supervisor, for his invaluable guidance, support and encouragement throughout this research project. I am also thankful to him for allowing me the freedom and creativity to solve problems in my own way.

I am also deeply thankful to Prof. Callum Hetherington and Texas Tech University for the use of their scanning electron microscope (SEM) and for their assistance and advice on the analysis of my samples. Their generosity and collaboration have greatly facilitated my work and enriched my learning experience.

I would like to acknowledge the University of Pretoria and the Material Science Laboratory for the use of their SEM, and for providing me with the necessary resources and facilities to conduct this research. I am grateful for the opportunity to pursue my academic goals at this institution.

I am indebted to Johan De Jager, the owner of the farm Duikerskrans, for granting me access to his land and allowing me to collect samples for this study. His cooperation and hospitality have been much appreciated.

Last but not least, I would like to thank my family and friends for their constant love, support and belief in me. They have been my source of motivation and inspiration throughout this journey. I dedicate this thesis to them.

ABSTRACT

The Upper Zone is the uppermost portion of the Rustenburg Layered Suite of the Bushveld Igneous Complex and has long been interpreted to have formed from the differentiation of a single magma pulse through closed-system fractionation. This is in contrast to theories proposed for the formation of the lower portions of the Bushveld, which state that multiple cycles of new magma injections occurred. In this study, the discovery of rocks believed to be igneous xenoliths in Subzone C of the Upper Zone in the Eastern Limb of the Bushveld Complex is investigated. The study area has not been extensively investigated in the past and the outcrops referred to in this study will be properly described for the first time. The xenoliths feature remnant trellis ilmenite exsolution textures that have not been observed elsewhere before. Extensive field work was conducted, as well as petrographical and geochemical analyses, that led to the conclusion that these foreign blocks were xenoliths of igneous origin. Furthermore, when geochemical and SEM data are analysed, the xenoliths show strong evidence of hydrothermal alteration and contain highly altered minerals, which the host rock does not, further solidifying the idea that these samples are, in fact, xenoliths. The presence of remnant ilmenite suggest that the xenoliths originated from magnetite-bearing units, and since the only magnetite-bearing units in the Bushveld Complex are found in the Upper Zone itself, this implies that the xenoliths originated from elsewhere in the Upper Zone. Therefore, it was concluded that they could be further classified as being autoliths. This directly challenges the single magma theory, since the presence of autoliths from the Upper Zone in subzone C suggests that at least one other magma pulse contributed to the formation of the Upper Zone, and thus the Upper Zone did not form in a closed system.

Keywords: Xenoliths; Bushveld Complex; Ilmenite; Trellis exsolution; Upper Zone

TABLE OF CONTENTS

<u>DECLARATION:</u>	<u>2</u>
<u>ACKNOWLEDGEMENTS.....</u>	<u>3</u>
<u>ABSTRACT</u>	<u>4</u>
LIST OF FIGURES	7
LIST OF TABLES.....	10
<u>CHAPTER 1: INTRODUCTION</u>	<u>11</u>
BACKGROUND TO THE RESEARCH PROBLEM	11
HYPOTHESIS, AIMS AND OBJECTIVES	12
GEOLOGICAL BACKGROUND.....	13
LITHOLOGY, HISTORICAL MAPS, AND PREVIOUS WORK IN THE AREA.	22
<u>CHAPTER 2: FIELDWORK DESCRIPTIONS</u>	<u>30</u>
SITE DESCRIPTION.....	30
FIELD WORK AND SAMPLING.....	32
FIELD RELATIONSHIPS	34
<u>CHAPTER 3: ANALYTICAL METHODOLOGY AND RESULTS</u>	<u>37</u>
LABORATORY TECHNIQUES.....	37
<u>PETROGRAPHY AND GEOCHEMISTRY</u>	<u>41</u>

GEOCHEMISTRY.....	47
ELEMENT MAPS.....	56
<u>CHAPTER 4: DISCUSSION.....</u>	<u>59</u>
THE GEOGRAPHIC SPREAD OF THE XENOLITHS	59
THE DISAPPEARANCE OF MAGNETITE	64
POSSIBLE ORIGINS.....	66
LIMITATIONS AND RECOMMENDATIONS	74
<u>CHAPTER 5: CONCLUSION</u>	<u>76</u>
<u>BIBLIOGRAPHY</u>	<u>78</u>
<u>APPENDIX</u>	<u>83</u>

LIST OF FIGURES

FIGURE 1- REGIONAL GEOLOGICAL MAP OF THE EASTERN LIMB OF THE BUSHVELD IGNEOUS COMPLEX, WITH THE RED STAR INDICATING THE LOCATION OF THIS RESEARCH. (ROSE ET AL., 2011)	13
FIGURE 2 – (A) STRATIGRAPHIC COLUMN SHOWING A SUMMARY OF THE SR-ISOTOPE VARIATIONS, THE DIFFERENT MAGMATIC STAGES AS WELL AS THE POSITIONS OF VARIOUS UNCONFORMITIES IN THE BUSHVELD COMPLEX WITH THE AREA OF INTEREST HIGHLIGHTED IN BLUE (AFTER (KRUGER, 1994)). (B) SECTION OF THE STRATIGRAPHIC COLUMN IN THE STUDY AREA, SHOWING SUBZONE C OF THE UPPER ZONE WITH THE AREA OF INTEREST HIGHLIGHTED IN BLUE. (MODIFIED AFTER (VON GRUENEWALDT, 1971)).....	17
FIGURE 3 – N-S CROSS SECTION OF THE BUSHVELD COMPLEX INDICATING THE LOCATION OF VARIOUS POSSIBLE FEEDER DYKES (KRUGER, 2005).....	18
FIGURE 4 - SCHEMATIC DIAGRAM OF DOUBLE-DIFFUSIVE CONVECTION (KRUGER & SMART, 1987).	19
FIGURE 5 - COARSE GRAINED ANORTHOSITIC PEGMATOID DISCOVERED ON DUIKERSKRANS (VON GRUENEWALDT, 1971). NOTE THE SHARP CONTACT WITH SURROUNDING MAGNETITE DIORITE (DARK).....	23
FIGURE 6 – B) PHOTOGRAPHS SHOWING WHAT IS DESCRIBED AS "RESORBED XENOLITHS" OF ANORTHOSITE INSIDE THE MAIN MAGNETITE LAYER IN THE ROOSSENEKAL AREA. C) ABUNDANT "IRREGULAR BODIES" OF ANORTHOSITE AT MAGNETITE LAYER 21 ON THE FARM PAARDEKLOOF TO THE SOUTH OF DUIKERSKRANS (SCOON AND MITCHELL, 2012).....	27
FIGURE 7 - (A) - SCANNED SECTION OF THE MAP BY (VON GRUENEWALDT, 1971) (B) - RECENT 1:50000 GEOLOGICAL MAP OF THE STUDY AREA WITH LEGEND (THOMAS, 2020). THE SECTION OF THE RIVER THAT WAS TRAVERSED IS INDICATED WITH THE RED DASHED LINE IN BOTH MAPS. (C) SCANNED SECTION OF THE GEOLOGICAL MAP PRODUCED BY (BOSHOFF, 1942).....	28
FIGURE 8 - SATELLITE IMAGES OF THE STUDY AREA. (A) A BROAD VIEW OF THE TOPOGRAPHY OF THE STUDY AREA SHOWING THE TAUTESHOOGTE MOUNTAIN PLATEAU AND THE MEANDERING STEELPOORT RIVER. (B) A SMALLER SCALE VIEW OF THE STEELPOORT RIVER IN THE STUDY AREA INDICATING THE POSITION OF OUTCROPS INSIDE AND ON THE BANKS OF THE RIVER (GOOGLE EARTH, 2021).....	31

FIGURE 9 - SATELLITE IMAGE OF THE SECTION OF THE STEELPOORT RIVER THAT WAS TRAVERSED INDICATING THE
OUTCROPS THAT WERE FOUND (GOOGLE EARTH, 2021)..... 32

FIGURE 10 PHOTOGRAPHS OF THE TYPES OF XENOLITHS IN THE SIX DIFFERENT CATEGORIES DESCRIBED ABOVE: FIGURE A)
CATEGORY A; FIGURE B) CATEGORY B; FIGURE C) CATEGORY C; FIGURE D) CATEGORY D; FIGURE E) CATEGORY E;
FIGURE F) CATEGORY F 36

FIGURE 11 - PHOTOMICROGRAPHS TAKEN FROM THE HOST ROCK SAMPLE SHOWING XPL IMAGES IN A) & c) AND
CORRESPONDING PPL IMAGES IN B) AND D). IN THESE IMAGES MOSTLY UNALTERED EUHEDRAL PLAGIOCLASE
CRYSTALS CAN BE SEEN WITH MINOR AMOUNTS OF INTERSTITIAL CPX AND THE OPAQUE MINERALS ARE
MAGNETITE. 42

FIGURE 12- FIGURES (A) AND (B) ARE PPL AND XPL PICTURES TAKEN IN THE HOST ROCK SAMPLE AA-01; FIGURE (C)
AND (D) ARE PPL AND XPL PICTURES TAKEN OF SAMPLE AA-09 WHICH SHOWS SERICITIZED PLAGIOCLASE;
FIGURES (E) AND (F) ARE PPL PICTURES FROM SAMPLE AA-11C SHOWING VEINS OF AMPHIBOLE CROSSCUTTING A
PLAGIOCLASE GRAIN. FIGURE (G) IS A PPL IMAGE OF SAMPLE AA-09 SHOWING FIBROUS GREEN AMPHIBOLE;
FIGURE (H) IS A PPL IMAGE FROM SAMPLE AA-11B SHOWING THE LARGE AMOUNT OF GREEN AMPHIBOLE AND
CHLORITE THAT IS COMMONLY OBSERVED..... 45

FIGURE 13- FIGURES A & B ARE BSD IMAGES SHOWING THE NORMAL TRELLIS EXSOLUTION OF ILMENITE WITHIN A
MAGNETITE GRAIN IN SAMPLE AA-01, THE HOST ROCK SAMPLE. FIGURE C, E, G & H ARE PHOTOMICROGRAPHS
TAKEN IN PPL AND 5X MAGNIFICATION, SHOWING THE REMNANT ILMENITE EXSOLUTIONS AND MAGNETITE
REPLACED WITH HORNBLLENDE AND CHLORITE FROM SAMPLES AA-09, AA-10B, AND AA-12 RESPECTIVELY.
FIGURE D IS A BSD IMAGE OF A REMNANT ILMENITE EXSOLUTION WITH HORNBLLENDE IN SAMPLE AA-09. FIGURE
F IS THE BSD IMAGE OF FIGURE E. 46

FIGURE 14 - XRD RESULTS VISUALISED AS A SERIES OF HISTOGRAMS..... 48

FIGURE 15 – (A) GEOLOGICAL MAP INDICATING THE LOCATION OF BK1, 2 & 3. (B) SIMPLIFIED STRATIGRAPHIC COLUMN
SHOWING WHERE THE BIERKRAAL DRILL CORES INTERSECT THE VARIOUS SUBZONES OF THE UZ (YUAN, 2017). 52

FIGURE 16 - MAJOR ELEMENT GEOCHEMISTRY COMPARISON OF THE COMPOSITION OF XENOLITHS TO THE COMPOSITION OF DRILL CORES TAKEN AT BIERKRAAL (BK1, 2 & 3) (YUAN, 2017). A) MgO vs FeO. B) MgO vs Al₂O₃ C) MgO vs CaO D) MgO vs Na₂O E) MgO vs SiO₂ F) SiO₂ vs FeO..... 53

FIGURE 17 - (A) TERNARY DIAGRAM OF PLAGIOCLASE, WITH THE HOST ROCK SAMPLE INDICATED IN THE RED SHADED AREA. (B) TERNARY SPINEL DIAGRAM INDICATING ILMENITE AND MAGNETITE FROM THE HOST AND THE XENOLITHS. (C) AMPHIBOLE CLASSIFICATION DIAGRAM (LEAKE ET AL., 1997)..... 55

FIGURE 18 - THE DISTRIBUTION OF CA-RICH VERSUS CA-POOR PLAGIOCLASE IN SAMPLE AA-06 IS ILLUSTRATED USING A BSD IMAGE (FIG (A)), FIGURE (B) IS AN ELEMENT MAP SHOWING THE DISTRIBUTION OF NA, FIGURE (C) IS AN ELEMENT MAP SHOWING THE DISTRIBUTION OF CA, AND FIGURE (D) IS A COMPOSITE ELEMENT MAP SHOWING THE DISTRIBUTION OF NA, CA, AL, FE AND TI. 58

FIGURE 19 - MAP SHOWING THE POSSIBLE EXTENT OF THE XENOLITHS (SHOWN IN RED), IF THEY ARE CONFINED TO A LAYER IN THE STRATIGRAPHY PARALLEL TO STRIKE..... 60

FIGURE 20 - BSD IMAGE FROM SAMPLE AA-11B SHOWING THE INTERGROWTH OF CLINOZOISITE WITHIN AN ALTERED PLAGIOCLASE CRYSTAL. THE TABLE ABOVE IS THE EDS DATA SHOWING WT% OF ELEMENT OXIDES..... 62

FIGURE 21 - TRELLIS EXSOLUTION OF ILMENITE OBSERVED IN MAGNETITE IN THE UPPER ZONE OF THE BUSHVELD IGNEOUS COMPLEX (VON GRUENEWALDT ET AL., 1985) 64

FIGURE 22 - Al/Ti RATIOS VS HEIGHT ABOVE THE PYROXENITE MARKER FOR BIERKRAAL SAMPLES IN THE WESTERN LIMB. GREEN, YELLOW AND BLUE SHADED AREAS REPRESENT THE Al/Ti RATIO INTERVALS FOR THE XENOLITHS SAMPLES AA-01, AA-06 AND AA-10B RESPECTIVELY. THE DASHED RED LINE INDICATES THE POSITION OF THE HOST ROCK IN THE STRATIGRAPHY. 71

FIGURE 23 - BOX AND WHISKER PLOT COMPARING THE Al CONTENT OF PLAGIOCLASE CRYSTALS IN WEIGHT% OXIDES BETWEEN ALL SAMPLES. IT IS SEEN THAT Al CONTENT VARIES GREATLY IN PLAGIOCLASE CRYSTALS FROM THE XENOLITH SAMPLES, BUT THE HOST ROCK (AA-01) HAS MUCH LESS VARIANCE. 73

LIST OF TABLES

TABLE 1-COMPARISON BETWEEN THE DIFFERENT DEFINITIONS OF SUBZONES IN THE UZ BASED ON THE APPEARANCE OF INDICATOR MINERALS ACCORDING TO DIFFERENT AUTHORS (SCOON & MITCHELL, 2012)	15
TABLE 2 – XRF RESULTS SHOWING THE MAJOR ELEMENT OXIDES IN EACH SAMPLE. SAMPLE AA-21-01 IS THE HOST ROCK SAMPLE, AND ALL OTHER SAMPLES ARE THE XENOLITHS.....	47
TABLE 3 – XRD RESULTS SHOWING MINERAL PHASES PRESENT WITHIN EACH SAMPLE. SAMPLE AA-21-01 IS THE HOST ROCK SAMPLE, AND ALL OTHER SAMPLES ARE THE XENOLITHS.....	48
TABLE 4 - RESULTS OBTAINED FROM ELEMENT MAP EFFECTIVE BULK COMPOSITIONS (EBC) COMPARED TO WHOLE ROCK BULK COMPOSITIONS OBTAINED WITH XRF	56
TABLE 5 - DESCRIPTION OF THIN SECTIONS INCLUDING THIN SECTION SCANS IN PPL	83
TABLE 6-TABLE SHOWING ALL SAMPLES THAT WERE COLLECTED IN THE FIELD ALONG WITH A BRIEF DESCRIPTION AND A PHOTOGRAPH	86

CHAPTER 1: INTRODUCTION

Background to the research problem

The Bushveld Igneous Complex is the world's largest layered igneous intrusion and, as such, has provided geoscientists around the world with a wealth of knowledge in the field of igneous petrology and economic geology. The Bushveld Complex covers an area of over 66 000 km², has a diameter of approximately 350 km, and has been extensively researched as an economic resource of PGMs. Despite being so well studied, the exact mechanism of formation of the Bushveld Complex is still disputed, and many uncertainties still exist regarding its origins. The Upper Zone of the Bushveld complex is the uppermost portion of the Rustenburg Layered Suite and is the setting for this research.

The study area is located in the Roossenekal area of the eastern Bushveld Complex, as shown in Figure 1, where a discovery of possible xenoliths in the Upper Zone was found outcropping in the Steelpoort River that flows through the farm Duikerskrans. Xenoliths are foreign fragments of rock that become entrapped in a body of magma. The mafic rocks of the Bushveld Complex are known to have occurrences of xenoliths in several places, for example, in the Northern Limb of the Bushveld, where xenoliths of the surrounding country rock as well as metasedimentary xenoliths can be observed in the host rock (Kinnaird et al., 2005). What makes the outcrops in this study unique is that they appear to host xenoliths of igneous origin, as well as metasedimentary xenoliths. The xenoliths appear in the field to be texturally distinct from the host material and, in some cases, have a well-defined boundary. There is also a noticeable variation in the shapes, sizes, and compositions between the xenoliths that have been discovered in this 500m outcrop in the Steelpoort River. The presence of these xenoliths raises questions as to where they originated and how their incorporation fits into models presented for the formation of the Upper Zone.

Little research has been done in this specific area of the Bushveld (Boshoff, 1942; Von Gruenewaldt, 1971; Scoon & Mitchell, 2012). The thesis of von Gruenewaldt (1971) provides an extensive investigation of the geological occurrences of a much broader geographic area that overlaps with the study area where the xenoliths were found. Von Gruenewaldt's study provides essential background information on the area but lacks a proper description and investigation of the outcrops of interest. More recent studies by Scoon & Mitchell did not focus on geological mapping of the area, but rather investigated a number of drill cores in order to analyse the broader geochemistry of the area. Previous research work was used to compare to the findings of this study, but it is worth noting that none of the previous research noted the presence of the outcrops investigated for this study. Therefore, the aim of this investigation was to properly characterise these outcrops by providing the petrographical and geochemical data.

Hypothesis, aims and objectives

The main hypothesis of this study theorises that the rocks discovered in the Upper Zone of the Bushveld Igneous Complex in the Roossenekal area can be categorised as xenoliths. On the contrary, the alternative hypothesis suggests that these occurrences cannot be classified as xenoliths and instead originated as a result of igneous processes.

The research aims for this investigation are twofold. Firstly, it seeks to enhance our understanding of the thermal history and metamorphic processes that influenced the formation of the Upper Zone. Secondly, it aims to contribute to a more comprehensive understanding of the mechanisms responsible for the incorporation of xenoliths into layered igneous intrusions.

To achieve these research aims, several specific objectives have been outlined. The first objective is to examine the differences in chemical compositions between the xenoliths

and the host rock using techniques such as X-ray diffraction (XRD), X-ray fluorescence (XRF), and scanning electron microscopy (SEM). The second objective is to conduct a petrographic analysis, with a focus on providing detailed descriptions of the textures of the xenoliths and making comparisons with the host rock. The third objective aims to offer a plausible explanation for the origin of the xenoliths within the Upper Zone of the Bushveld Igneous Complex in the Roossenekal area.

Geological background

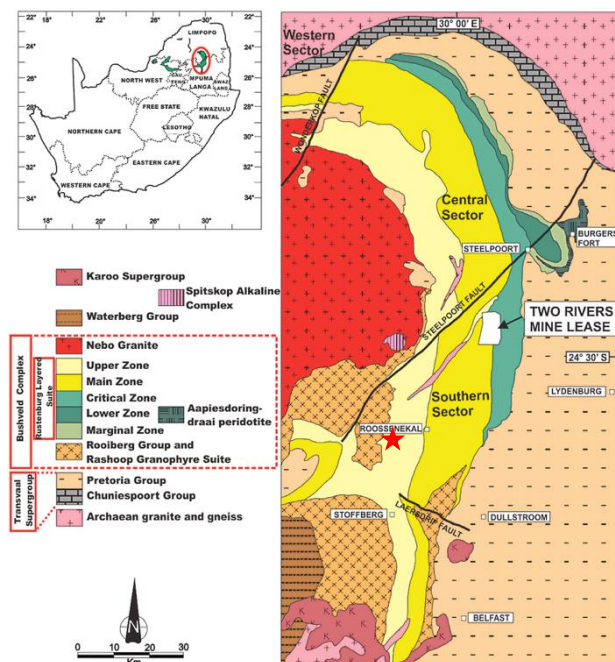


Figure 1- Regional geological map of the eastern limb of the Bushveld Igneous Complex, with the red star indicating the location of this research. (Rose et al., 2011)

The Bushveld Igneous Complex is widely known to be the largest layered igneous province in the world. The Bushveld Complex was formed approximately 2 billion years ago and comprises of a bimodal mostly mafic and minor felsic composition; however, the tectonic setting for the magmatism is highly debated (Eales & Cawthorn, 1996).

The Bushveld Complex lies within the Transvaal basin, which comprises a 12 km thick succession of clastic and chemical sedimentary rocks (Von Gruenewald, Sharpe, et al., 1985). The stratigraphy of the Bushveld has been divided into the Rustenburg Layered Suite, the felsic Roshoop Granophyre Suite and the Lebowa Granite Suite, of which the Rustenburg Layered Suite is of most geological and economical significance. These units can also be seen in the geological map in Figure 1. The

emplacement of these units was proven to have occurred over a very short period of time and were formed mostly synchronous from approximately 2060 to 2055 million years ago (Ma) (Harmer & Armstrong, 2000; Mapeo et al., 2004). The peak period of magma flux occurred around 2055–2056 Ma (Scoates et al., 2021). Unlike a single, progressively filled and cooled magma chamber, the U–Pb zircon crystallization ages within the complex do not exhibit a continuous systematic decrease from the base to the top. Instead, the lower section of the Bushveld Complex evolved through successive intrusions and the accretion of sheet-like intrusions (sills), occurring at different stratigraphic levels. The crystallization of the primary volume of the complex, represented by the thick gabbroic sequences in the Main Zone and Upper Zone, was confined to a relatively narrow time interval of approximately 1 million years, centred around 2055–2056 Ma (Scoates et al., 2021). The most recent igneous activities in the Bushveld Complex involve granites and granophyres in the roof, along with a diorite in the uppermost Upper Zone, occurring around 2055 Ma (Maier et al., 2013).

The Rooiberg volcanics unconformably overlies the Rustenburg Layered Suite (RLS) and represents the volcanic expression of the same magmatic event that produced the RLS (Lenhardt & Eriksson, 2012). The Rooiberg volcanics are mostly felsic in composition, ranging from basalt to rhyolite, and are thought to have resulted from the fractional crystallisation of the bushveld magma .

When magma intruded as sills into the Transvaal sedimentary sequence and below the extrusive Rooiberg volcanics (Eales & Cawthorn, 1996) the intrusion of these large volumes of mafic magma led to the formation of the Rustenburg Layered Suite, which is a laterally extensive mafic layered intrusion and is divided into a number of different zones. The Marginal Zone is found around the edge of the intrusion whereas from the base of the complex up are the Lower Zone, the Critical Zone, the Main Zone and lastly the Upper Zone.

The Bushveld Complex is underlain by the Transvaal sedimentary sequence and overlain by Rooiberg, Waterberg and the Karoo sediments. The geological map shown in Figure 1 indicates the Eastern Limb of the Bushveld Complex, more specifically the Rustenburg Layered Suite, with the area of interest for this study marked with the red star.

Of interest for this study is the Upper Zone (UZ) of the Rustenburg Layered Suite. The UZ is most known for hosting around 25 magnetite layers hosted in various mafic units of anorthosite, ferro-gabbro, and norite. The Upper Zone has been subdivided into various subzones based on mineral appearances. The subzones have been divided into four groups, from Subzone A to Subzone D, in certain studies (Von Gruenewaldt, 1971), but other authors have used a three-fold division, from Subzone A to Subzone C (Scoon & Mitchell, 2012; Yuan et al., 2017). The main differences between the classification of the subzones can be seen in Table 1. Subzone A (UZa) is generally described as the zone above the first appearance of cumulus Ti-magnetite, Subzone B (UZb) as the first appearance of cumulus olivine, and Subzone C (UZc) as the first appearance of cumulus apatite. This study will also make use of the threefold division and is focused on UZc below magnetite layer 21 and in the magnetite gabbro units highlighted in blue in Figure 2(b). This would be conformable with Subzone D that is referred to in earlier papers (Von Gruenewaldt, 1971)

Table 1-Comparison between the different definitions of subzones in the UZ based on the appearance of indicator minerals according to different authors (Scoon & Mitchell, 2012)

Scoon and Mitchel, 2012	Von Gruenewaldt, 1973	Wager and Brown, 1968
Subzone E	Subzone D	Subzone C
Upper contact of upper magnetite layer 21	Appearance of Cumulus Apatite	Appearance of Cumulus Apatite
Subzone D		
Appearance of Cumulus Apatite	Subzone C	Subzone B
Subzone C		
Appearance of Cumulus Olivine		

	Appearance of Cumulus Olivine	Appearance of Cumulus Olivine
Subzone B	Subzone B	Subzone A
Geochemical transition approximately 80 m below MML	Layer Contact of MML	Lower contact of lower magnetite layer 1
Subzone A	Subzone A	
Appearance of Cumulus Ti-Magnetite	Appearance of Cumulus Ti-Magnetite	

The units below the UZ, namely the Critical, Main, and Lower zones, are thought to have formed from the injection of a variety of different magma pulses. The formation of the UZ, however, remains disputed, and there are various different theories that have been put forward. One popular theory speculates that the UZ may have differentiated from a single magma chamber (Kinnaird et al., 2002; Kruger, 1994; Tegner et al., 2006; Van Tongeren & Mathez, 2013). This is illustrated in Figure 2 (a) where the cyclic variation of the $^{87}\text{Sr} / ^{86}\text{Sr}$ isotope ratio in the lower part of the stratigraphy is classified as the integration phase, and the uniform Sr isotope ratio in the upper part is classified as the differentiation stage. Generally, an increase in the Sr isotope ratio indicates the addition of an enriched melt that has been contaminated by the crust, whereas a decrease in the Sr isotope ratio indicates the addition of a more depleted mantle-derived melt.

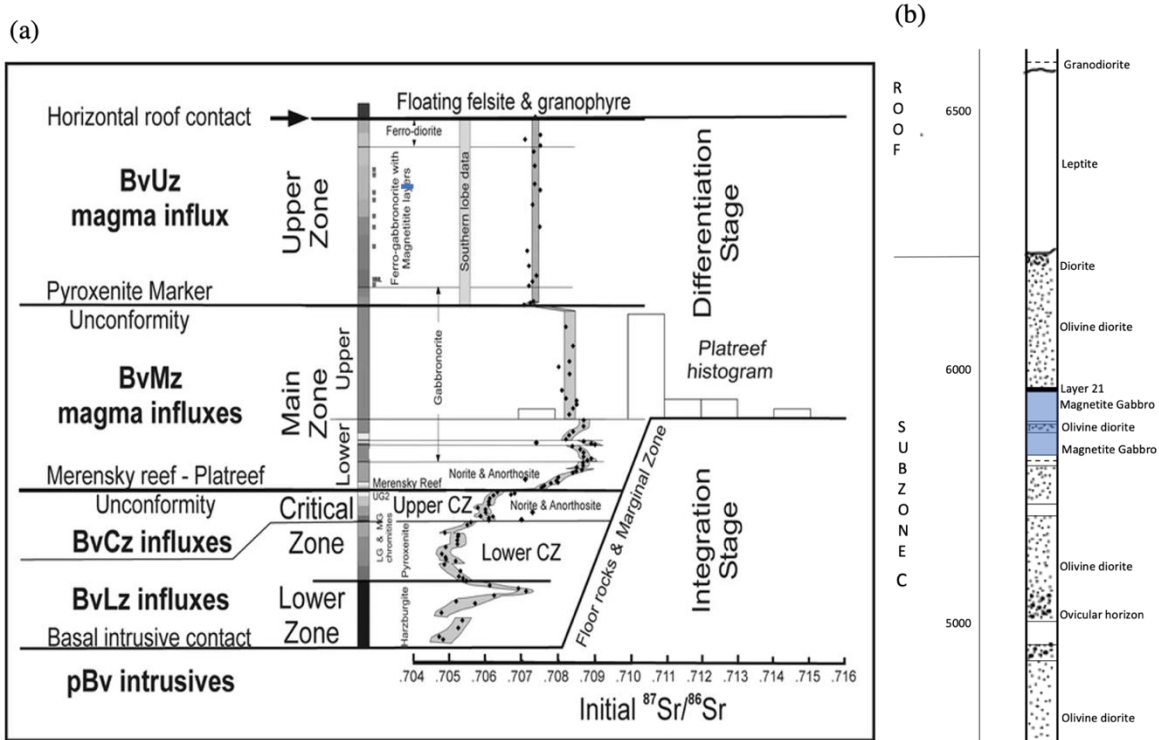


Figure 2 – (a) Stratigraphic column showing a summary of the Sr-isotope variations, the different magmatic stages as well as the positions of various unconformities in the Bushveld Complex with the area of interest highlighted in blue (after (Kruger, 1994)). (b) Section of the stratigraphic column in the study area, showing Subzone C of the Upper Zone with the area of interest highlighted in blue. (modified after (Von Gruenewaldt, 1971))

This variation between lower and higher Sr ratios is present in the lower part of the stratigraphy and is part of the integration phase. When the Sr isotope ratio remains constant, it is an indication that no new magma has been added (Kruger, 2005). The uniform Sr isotope ratio that can be observed in the Upper Main Zone and above the Pyroxenite Marker has been used to argue that the UZ did not experience any new influxes of magma and that the entire UZ is the product of in situ fractional crystallisation in a closed system (Kruger, 1994; Tegner et al., 2006; Van Tongeren et al., 2010). The Upper Main Zone is also considered to be highly differentiated; however, the last major injection of magma is speculated to have occurred at the level of the Pyroxenite Marker unconformity. This can be seen in Figure 2 (a) where there is a sudden decrease in the Sr isotope ratio at the level of the Pyroxenite Marker, and after this event no more additional magma injections can be recognised in the Sr isotopic system.

Overall, the Rustenburg layered suite has been described as possibly experiencing four major magmatic injection events, each of which caused an unconformity in the sequence (Kruger, 2004; Tegner et al., 2006). These magmatic injections occurred via three magmatic conduits responsible for the injection of source magmas from different lineages (Kruger, 2004). The first lineage is the BvLz magma responsible for the crystallisation of the Lower Zone. Similarly, the BvCz magma influx was responsible for the formation of the Critical Zone, the BvMz for the Main Zone, and the BvUz for the Upper Zone. Figure 3 is a N-S cross section of the Bushveld Complex, showing the possible locations of each feeder dyke responsible for the injection of each lineage. Each of these new major magma influxes caused the vertical and lateral expansion of the magma chamber and also caused the formation of unconformities at the base of the new intrusion. The Merensky Reef and the Pyroxenite Marker mark the base of these unconformities in the sequence. A large amount of new liquid

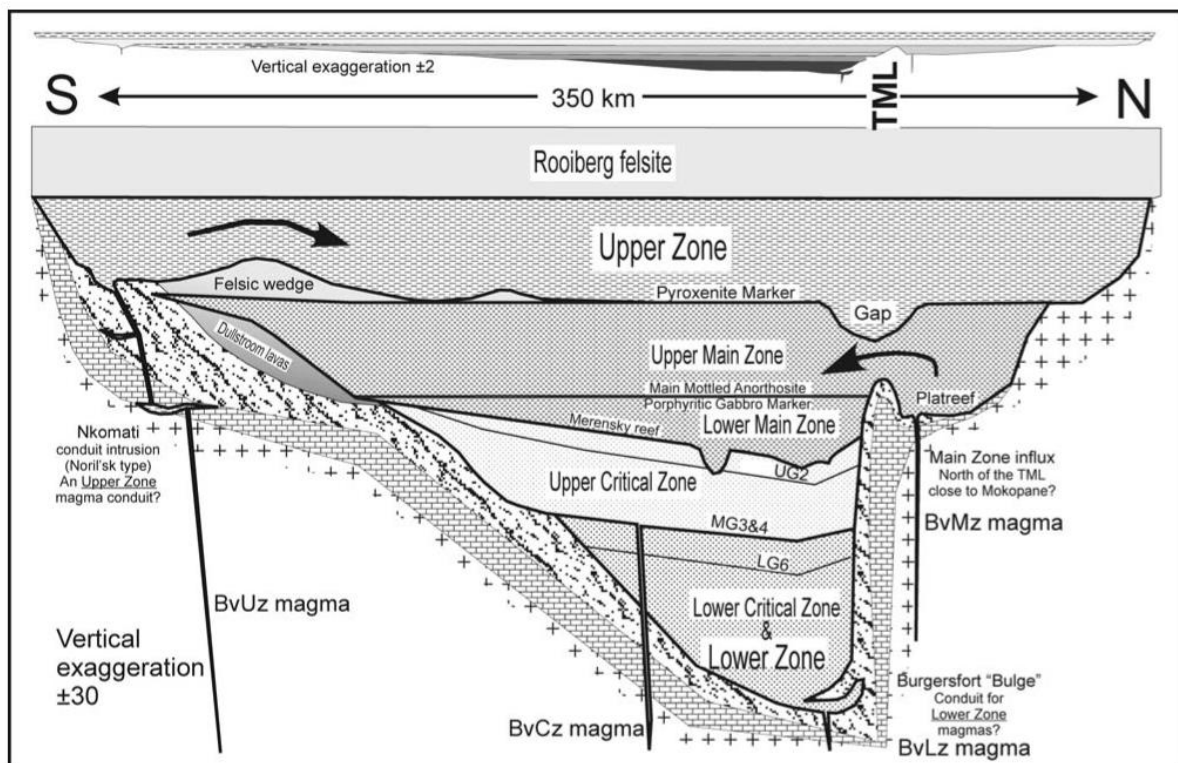


Figure 3 – N-S cross section of the Bushveld Complex indicating the location of various possible feeder dykes (Kruger, 2005)

being added to the chamber resulted in magmatic erosion and solution of the cumulate pile on the floor, thus creating the unconformity in the sequence (Kinnaird et al., 2002). The reaction of the new liquid with the cumulate pile also resulted in the precipitation of the Merensky Reef and the Pyroxenite Marker at the base of the new intrusions (Kruger, 1994). The third major unconformity in the sequence can be observed at the boundary between the Bushveld Complex and the Transvaal sediments. This is how the position of major unconformities can be an indication of the injection of large new magma pulses into the system (Kruger, 1994).

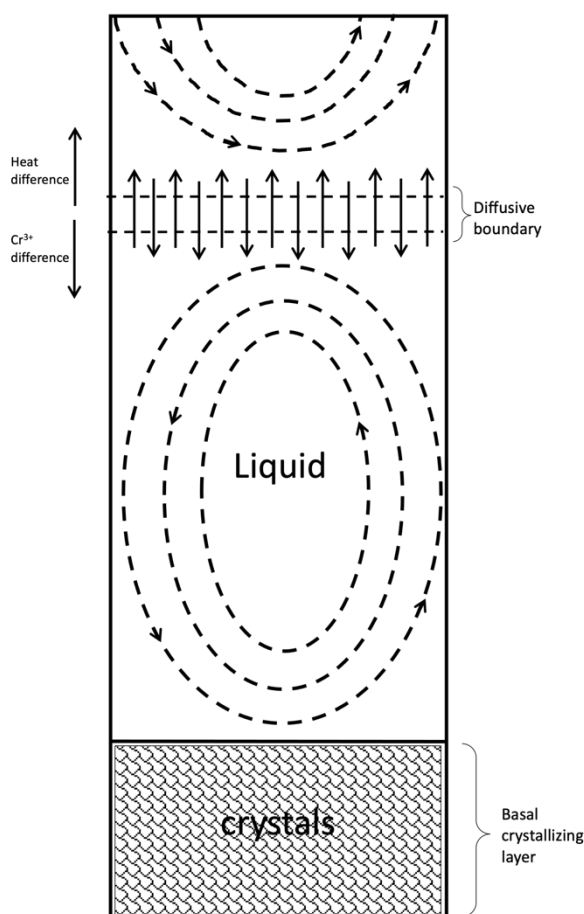


Figure 4 - Schematic diagram of double-diffusive convection (Kruger & Smart, 1987).

The theory of double-diffusive convection has also been suggested for the formation of the UZ and would go hand in hand with the Sr isotopic evidence mentioned thus far. Double-diffusive convection (d.d.c.) is a type of fluid motion that occurs when there are two types of density gradients in a fluid that act in opposite directions. Density gradients are caused by differences in temperature and composition in the magma (Irvine et al., 1983). If one assumes that the UZ was injected as one single pulse of magma, d.d.c. could have played an important role in its formation, since layered intrusions such as

the Bushveld Complex can be stratified in the liquid state by the process of d.d.c. (Kruger & Smart, 1987) The magma of the UZ can be described as a magnetite-liquid system with a very large density contrast between magnetite and liquid. Thus, fractional crystallisation of

magnetite from this system could be the driving force behind the instability required to produce double-diffusive convection. As the UZ magma cooled, the minerals began to crystallise, leading to differences in composition and density gradients. The hot, less dense material rose and the cooler, more dense material sank, resulting in the mixing and movement of magma in the chamber. This mixing allowed for the concentration of minerals and magnetite was assumed to have crystallised at the base of the lowermost layer of the d.d.c. system. The 5 km thick cumulate floor at the base of the UZ was believed to have prevented downward heat loss and could even have supplied heat to the liquid UZ, aiding further in convection (Kruger & Smart, 1987).

Some theories about UZ formation do not support the idea that the UZ was created from a single large magma chamber. Whole rock geochemical data collected from the UZ in the Eastern Limb in the Roossenekal area have been found to be inconsistent with a closed system fractionation hypothesis (Scoon & Mitchell, 2012). Though the uniform Sr isotope ratios observed in the UZ have interpreted to be an indication of closed system fractionation (Kruger et al., 1987; Tegner et al., 2006; Van Tongeren & Mathez, 2012), a uniform Sr isotopic ratio does not necessarily preclude the possibility of multiple isotopically homogenous magma influxes (Scoon & Mitchell, 2012). Scoon & Mitchell (2012) argued that it would be implausible for such a laterally extensive and thick sequence like the Upper Main and Upper Zones to have formed from a single pulse of magma, as it would have destabilised the underlying older components of the Bushveld Complex. An alternative theory was presented that suggested that the UZ could have formed from numerous magma pulses, each new pulse associated with the formation of a new magnetite layer or group of layers (Scoon & Mitchell, 2012). A similar finding was made by (Ashwal et al., 2005) in which numerous geochemical reversals and discontinuities in mineral compositions were observed in drill core

data from Bellevue in the Northern Limb. These findings were interpreted to be representative of new magma additions and also challenged the closed-system model.

Another study focussed on the petrography and geochemistry of the UUMZ analyses 2.1 km of drill cores from Bierkraal in the Western Limb (Yuan et al., 2017). Sampling for this study was done at <10 m intervals in order to create a more detailed geochemical profile. The geochemical data from this study indicated that magma replenishment probably occurred in the UUMZ. It was concluded that although the samples exhibit a broad fractionation trend, a series of compositional reversals in the anorthite content of plagioclase, Mg# in pyroxenes and olivine, and Cr in magnetite are observed. Most of these reversals are correlated with the absence of cumulus minerals (pyroxene, olivine, apatite, Fe–Ti oxides) or the appearance of monomineralic layers. These reversals are used as boundaries to divide the UUMZ into 18 cycles. Consequently, the study concludes that the UUMZ cumulates were not formed by closed-system differentiation but more likely crystallised from a series of magma pulses (Yuan et al., 2017).

The models of formation previously presented for the emplacement of the Upper Zone are instrumental in understanding the findings of this project. The single magma theory referenced most frequently in the literature postulates that the UZ magma was incorporated into the magma chamber and subsequently mixed with residual material and further differentiated in situ without any further addition (Cawthorn, 1994; Kinnaird et al., 2002; Kruger, 1990, 1994; Tegner et al., 2006; Van Tongeren & Mathez, 2012). The well-defined and abundant layering of magnetite in the Upper Zone is also believed to have evolved from this well mixed magma (Kruger, 1987). Furthermore, the UZ has long been speculated to be the crystallisation product of the last major melt injection into the bushveld magma chamber (Yuan et al., 2017). However, there has been some evidence that the UZ magma chamber may

not have been a closed system and experienced numerous influxes of isotopically homogeneous magma pulses (Ashwal et al., 2005; Scoon & Mitchell, 2012; Yuan et al. 2017). The findings of this project will ultimately serve to contribute or detract from one of these theories.

Lithology, Historical maps, and previous work in the area.

The Upper Zone is a thick and laterally extensive sequence of differentiated, iron-rich cumulates. This includes the Main Magnetite Layer, the largest vanadium-rich Ti-magnetite layer in the world (Von Gruenewaldt, 1971). The Upper Zone is further notable for its layering of dark dense magnetite with considerably less dense light-coloured anorthosite layers. Despite the layers of magnetite and anorthosite, the dominant lithology consists mostly of homogeneous poorly layered ferrogabbro which progresses towards magnetite-olivine gabbro further upward in the succession (Von Gruenewaldt, 1971; Wager & Brown, 1968; Willemse & Visser, 1969). The uppermost part of the succession above the Layer 21 magnetite is composed of olivine diorite and diorite, as can be seen in the stratigraphic column in Figure 2 (b).

The study area is located 13 km south-west of Roossenekal in Limpopo where the Steelpoort river runs through the Duikerskrans farm. The geology of this area was extensively mapped by (Boshoff, 1942) and Von Gruenewaldt (1971). The geological map produced by Von Gruenewaldt was the last geological map produced of the area and is still used as the primary reference for recent maps. The most recent geological map available for the study area can be seen in Figure 7(b) (Council for Geoscience, 2021). This geological map does not indicate any outcrops in the Steelpoort River where the rocks in this study are being investigated. Instead, the area is mapped only as alluvium, referring to the river sediments.

The outcrops around the study area are mapped as olivine diorite, interlayered magnetite gabbro, and anorthosite forming part of the Luiperdshoek Olivine Diorite (Rlui) of the Roossenekal Subsuite (Rrs) of the Upper Zone. The outcrops found within the river bed are not present on these maps.



Figure 5 - Coarse grained Anorthositic pegmatoid discovered on Duikerskrans (Von Gruenewaldt, 1971). Note the sharp contact with surrounding magnetite diorite (dark).

The thesis of von Gruenewaldt provides an extensive investigation into the geological occurrences of a much broader geographical area, but this overlaps with the study area where the proposed xenoliths were found. von Gruenewaldt's thesis provides some insight into the petrographical and mineralogical background of the study area. This work has described a specific rock type in the Duikerskrans study area that could be related to the outcrops of interest for this study. The rocks are described as coarse-grained anorthositic rocks occasionally encountered in subzones C and D and are pictured in Figure 5. Von Gruenewaldt further explains that these "pegmatoids" appear to have no relation to the layered sequence in which they are found and also do not have a preferred orientation. The mineralogy of these

rocks is described as being dominated by large anhedral crystals of plagioclase with intercumulus green hornblende. Two of these specimens were reportedly found, one of which is visible on the map in Figure 7 (a), the numbered specimen G232. It was speculated at the time that these pegmatoids could have formed as a result of a concentration of volatile-rich intercumulus liquids and the emplacement of these into higher horizons. If this was the case, then the plagioclase is expected to be enriched in albite.

Of particular interest is the fact that this specimen was found only a few hundred metres away from where the outcrops in this study were found, and also appears to be below the layer 21 magnetite. Unfortunately, there was no geochemical analysis on these samples, which makes a direct chemical comparison not possible. Furthermore, Von Gruenewaldt does not mention the appearance of any xenoliths in the study area, despite the extensive and thorough mapping that was conducted. It is also possible that the outcrops in this study were not previously observed, due to their position in and around the Steelpoort River, which could have had a higher water level at the time of previous mapping projects, obscuring the outcrops from view.

The work done by (Boshoff, 1942) provides less insight into petrography and mineralogy, but nevertheless provides valuable and detailed accounts of geological occurrences in the study area. In the map in Figure 7 (c), the positions of a number of calc-silicate xenoliths are indicated on the map. This is noteworthy since this is the only geological map of the study area that indicates the presence of these xenoliths. The size is described as at least 100 m in diameter, which is much different from the outcrops described in this study. These large xenoliths seem to be consistent with other metasedimentary xenoliths that have been observed in the UZ. Large metasedimentary xenoliths like these have been found in various other locations, most notably in the Northern Limb above the Platreef (Kinnaird et al.,

2005), but also in the Eastern Limb near Magnet Heights (Molyneux, 1970; Wallmach et al., 1989) and various other locations. They are commonly believed to be fragments of the surrounding Transvaal sediments that have been incorporated into the Bushveld magmas during emplacement (Eriksson et al., 1995). Large metasedimentary xenoliths such as these are sometimes referred to as sedimentary rafts. The occurrence of the calc-silicate xenoliths on Duikerskrans provides more geological context and serves to illustrate the contrast between the xenoliths that are usually found in the UZ and the rocks that are studied for this project.

Another notable study conducted in the study area investigated the geochemical stratigraphy of the UZ by analysing several drill cores taken around the Roosenekal area (Scoon & Mitchell, 2012). This study was based on data from a fence of five drill cores that provided coverage of the entire UZ (2300m) and a part of the Upper Main Zone. Whole rock geochemical analyses was performed for a suite of samples covering the entire sequence at a height interval of 20 m. Across the five drill cores, a total of 163 samples were taken and whole rock analysis was performed for the major and trace elements using standard XRF methods. The whole rock Mg # was used as the main method to examine upward differentiation trends, and it was found that the scatter in the data was not consistent with closed-system fractionation, but rather more consistent with magma recharge in the UZ. Samples in the Upper Main Zone were observed to have Mg# values much higher than those observed in the lower part of the UZa, which could be evidence in support of a break at the base of the UZ. In general, Mg#s in UZa through UZc showed repeated evidence of reversals and only minor fractionation. Interestingly, UZd (conformable to UZc in this study) revealed evidence of a persistent differentiation trend that is then broken by a sequence of reversals toward the top. These trends are also supported by variations in some trace elements. The variation of Zr and Y with height was also examined, which revealed an absence in

fractionation in UZa through UZd. This study by Scoon & Mitchell concluded that the geochemical reversals were evidence of multiple magma influxes in the UZ. Furthermore, it is speculated that the UZ could have differentiated from an entirely different lineage of magma, possibly an iron-rich tholeiite, which deposited the characteristic layers of Fe-Ti oxides each time a new pulse of magma was injected.

Interestingly, the study notes the presence of “resorbed xenoliths” of anorthosite that were found in magnetite layers, as can be seen in Figure 6 (a). Furthermore, the study also discovered what was described as irregular bodies of anorthosite that have been flattened parallel to the layering and also show scalloped edges, as can be seen in Figure 6 (b). These bodies were not investigated further; i.e. they were not sampled or analysed in any way. Once

again, this more recent study also did not note the outcrops that were investigated for this project, even though sampling was also done on the Duikerskrans farm.

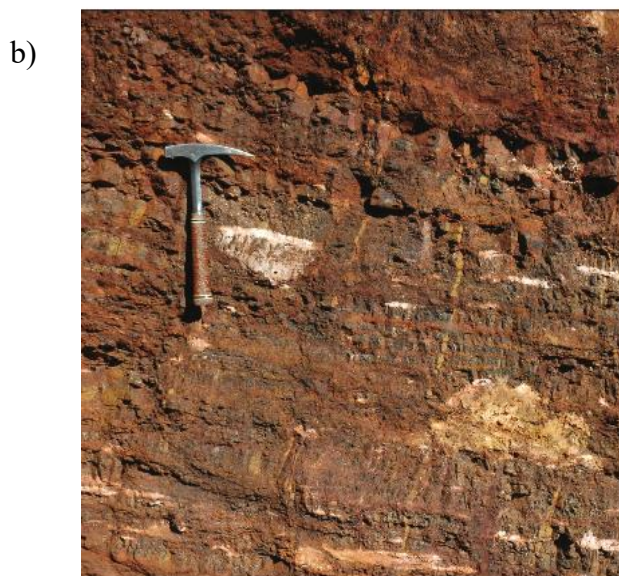
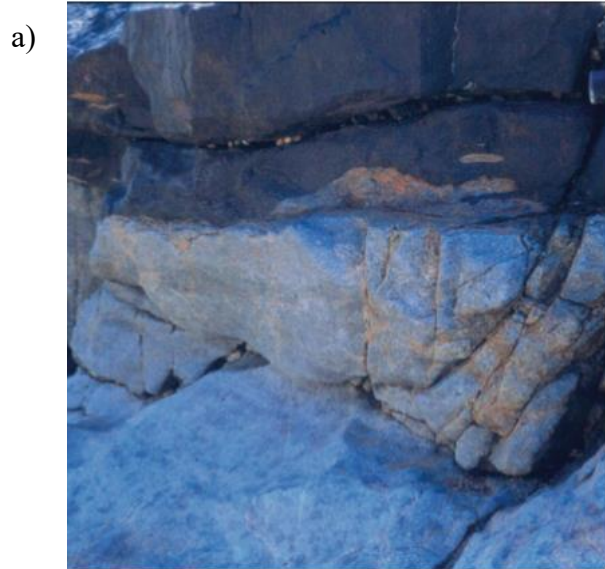


Figure 6 – a) Photographs showing what is described as "resorbed xenoliths" of anorthosite inside the main magnetite layer in the Roosenekal area. b) Abundant "irregular bodies" of anorthosite at magnetite layer 21 on the farm Paardekloof to the south of Duikerskrans (Scoon and Mitchell, 2012)

The works of previous researchers in the Roosenekal area provided a lot of contextual information in order to critically analyse the findings made in this project. The description of irregular bodies in the host rock is noteworthy in two of the previous studies (Scoon & Mitchell, 2012; Von Gruenewaldt, 1971), whereas the other study describes the appearance of calc-silicate xenoliths in the vicinity of the study area (Boshoff, 1942) None of

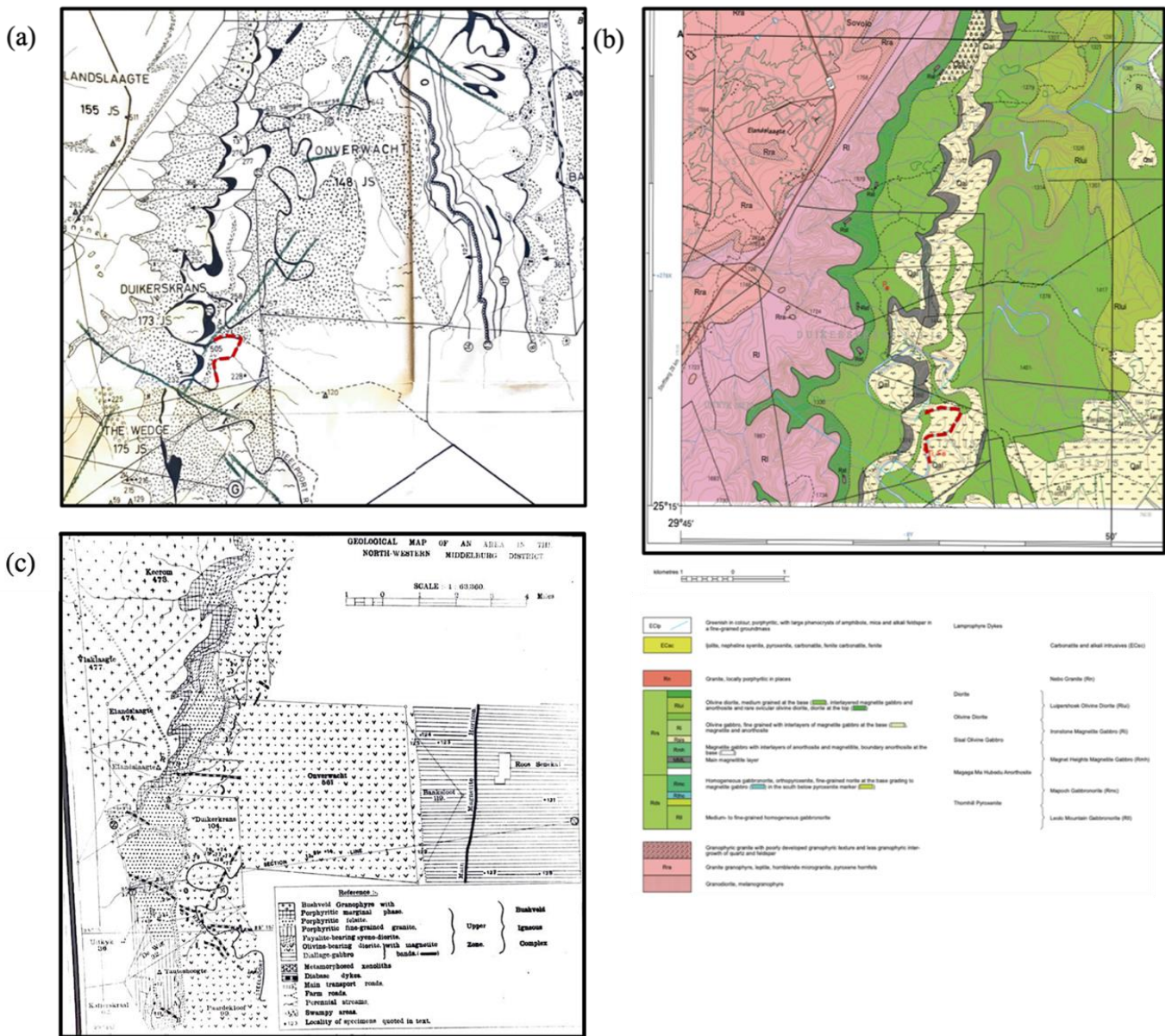


Figure 7 - (a) - Scanned section of the map by (Von Gruenewaldt, 1971) (b) - Recent 1:50000 geological map of the study area with legend (Thomas, 2020). The section of the river that was traversed is indicated with the red dashed line in both maps. (c) Scanned section of the geological map produced by (Boshoff, 1942).

the previous works in the area have sampled or analysed these occurrences and do not discuss them at length. Furthermore, none of the previous studies makes any mention of the outcrops being investigated for this project, which means that their presence was not previously taken into account when formulating models for the formation of the UZ.

CHAPTER 2: FIELDWORK DESCRIPTIONS

Site Description

The broad topography of the region can be described as a flat plateau with gently undulating slopes that are deeply incised by tributaries of the Steelpoort and Blood rivers that lead into a wide valley below. The edge of this plateau is defined by steep slopes formed by the contact between the felsic roof rocks above and the mafic gabbroic rocks of the UZ below. The lower lying regions surrounding the plateau are dominated by UZ material and host the meandering Steelpoort river east of the plateau.

The Steelpoort River runs through the Duikerskrans farm, as seen on the map in Figure 8 and provides excellent exposure of the magnetite gabbro outcrops that are investigated for this project. The outcrops of interest are located in Subzone C (UZc) of the Upper Zone and are hosted in the magnetite gabbro units visible in the stratigraphic column in Figure 2. The river runs roughly parallel to strike in this particular region, making it possible to follow the river upstream for a few hundred metres along strike. Most of the outcrops investigated were located inside or on the immediate banks of the river, as seen in Figure 9, which makes sampling locations somewhat limited. In fact, if the river water level only rose by a few metres, the outcrops would no longer be accessible or visible above the water.



Figure 8 - Satellite images of the study area. (a) A broad view of the topography of the study area showing the Tauteshoogte mountain plateau and the meandering Steelpoort river. (b) A smaller scale view of the Steelpoort river in the study area indicating the position of outcrops inside and on the banks of the river (Google Earth, 2021)

Field Work and Sampling

The field work for this project consisted of a combination of field mapping and observations, as well as sampling. One of the objectives in the field was to attempt to map the full extent of these outcrops, as far as possible, given the rough terrain and fenced portions of land that we were not given permission to enter. Another objective was to try to describe field relations of these outcrops and to try to establish a grouping or pattern. The last objective was to obtain samples of these outcrops to conduct petrographical and geochemical analysis.

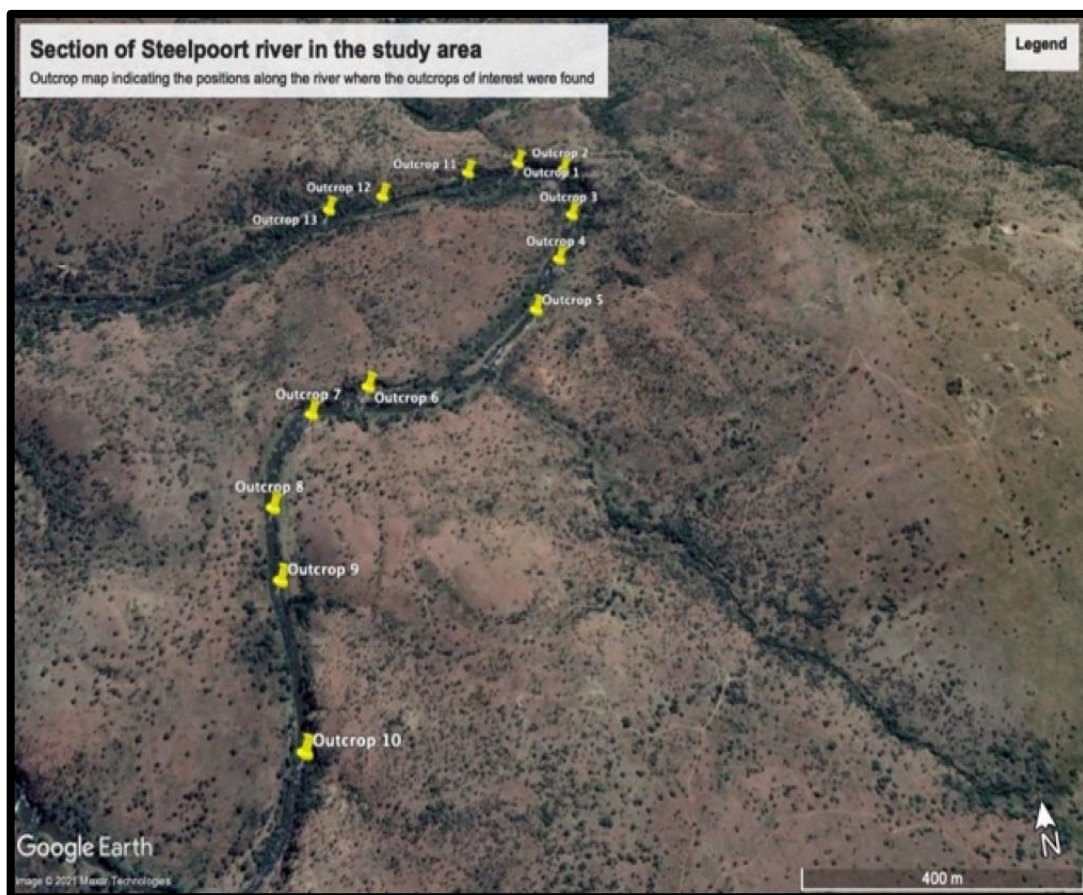


Figure 9 - Satellite image of the section of the Steelpoort river that was traversed indicating the outcrops that were found (Google Earth, 2021).

To try to determine the extent of these outcrops, a traverse of the Steelpoort River on Duikerskrans was carried out. A section of the river of about 2 km was traversed to observe all outcrops of interest, as can be seen in Figure 9. The river was followed upstream until the

occurrences became fewer and nearly non-existent around the location of outcrop 10. At this point, the river also became much harder to follow due to the deep water levels that were difficult to cross and the steep cliffs on either side. During this traverse, the outcrops were examined in detail to determine field relationships and implement a rough classification of the occurrences.

The sampling technique used in this study consisted of non-probability sampling, as the sampling was based on the discretion of the researcher. More specifically, a judgment sampling technique was implemented. The justification for this is that the sample size for this investigation was limited and not all samples were easily accessible. The samples chosen for analysis were chosen so that a sample of each different type of occurrence was included. Another factor that determined whether or not a sample was chosen was the size of the occurrence and its ability to be accurately sampled. This was a factor because the samples were taken with a handheld core drill and due to the location of the sampling area on the banks of the river, not all occurrences could be easily sampled. It was also not practical to transport the core drilling machine on the entire traverse along the river, meaning that all samples were taken in relatively close proximity. This introduces some degree of unavoidable bias into the investigation, but an attempt was made to mitigate this by sampling different types of occurrences.

After the appropriate samples were chosen, they were then sampled using a handheld core drilling machine. The drilling machine was able to penetrate to a depth of approximately 20 cm, but most of the cores that were extracted were between 5 and 10 cm in length with a diameter of 3 cm. The core samples were then placed in sample bags and appropriately labelled. In total, 16 samples were collected in the field for further analysis. These samples

are described in Table 6 in the appendix and include sample numbers, brief descriptions, and photographs.

Field relationships

The field work portion of the study involved a detailed inspection of the study area by performing a series of traverses up and downstream the Steelpoort river to describe any field relationships. Initially, the outcrops containing the xenolithic bodies were only discovered in one isolated section of the Steelpoort River (outcrop 1 in Figure 9). After thorough mapping of the area, more of these outcrops were discovered further up and downstream from the original site. Ultimately, enough xenoliths were observed to categorise them into six distinct groups. These categories are based on physical appearance and do not take into account factors like geochemistry since this was based on field observations.

Category A xenoliths (Figure 10 (a)) can be described as being mostly composed of plagioclase, and thus light in colour with interstitial, anhedral hornblende crystals. There is also a sharp contact visible with the host rock. Category A bears many similarities to what was previously described as an anorthositic pegmatoid (Von Gruenewaldt, 1971), but was also the category that was the least abundant in the field.

Category B (Figure 10 (b)) consisted of rocks with a well-defined plagioclase rim area with a sharp contact with the host rock and a coarse-grained core composed of large euhedral plagioclase crystals with interstitial hornblende. Most of the occurrences in this category have a rounded to subrounded shape and can be from 10cm to 90cm in diameter. This category was much more commonly observed than Category A.

Category C (Figure 10 (c)) has a characteristic plagioclase rim area that can be between 3 and 5 cm thick. The core consists of a darker material; however, there are no defined crystal shapes visible in the core. There is also a sharp contact with the host rock.

Category D (Figure 10 (d)) consists of hornblende, with a much finer grained plagioclase than category B. The contact with the host rock is gradual and consists of a lighter grey material. This category often has a well-defined shape, either angular or round (as opposed to a deformed shape), with a large diffuse light grey rim area.

Category E (Figure 10 (e)) is very different from the other xenoliths because these rocks appears more silicic or metasedimentary in composition. This is due to the characteristic banding of light and dark material giving a layered appearance. The rocks in this category are often rectangular or subangular in shape, has no visible crystals, and has a well-defined sharp contact with the host rock. The contact is often also marked by a thin layer of dark minerals. The occurrences in this category are usually only between 20 and 30 cm in length and 10 to 20 cm in width.

Category F (Figure 10 (f)) is similar to category E due to the presence of distinct layering and seems to have a similar mineral composition, however, is categorised separately. This is because the rocks in this category are usually much larger than category E and commonly have a very elongated and deformed appearance. The banding is heavily deformed and has an almost gneissic appearance. Rocks in this category can have occurrences that are up to 3m in length and about 20cm wide. There is also a sharp contact with the host rock.

Numerous occurrences were observed in each category in the field, although not every specific occurrence was documented. Instead, the outcrops were mapped and the occurrences found in each outcrop were classified into a category. For the purposes of limiting this study, only the xenoliths of igneous origin were analysed and investigated, i.e., categories E and F are not included in the rest of the study.

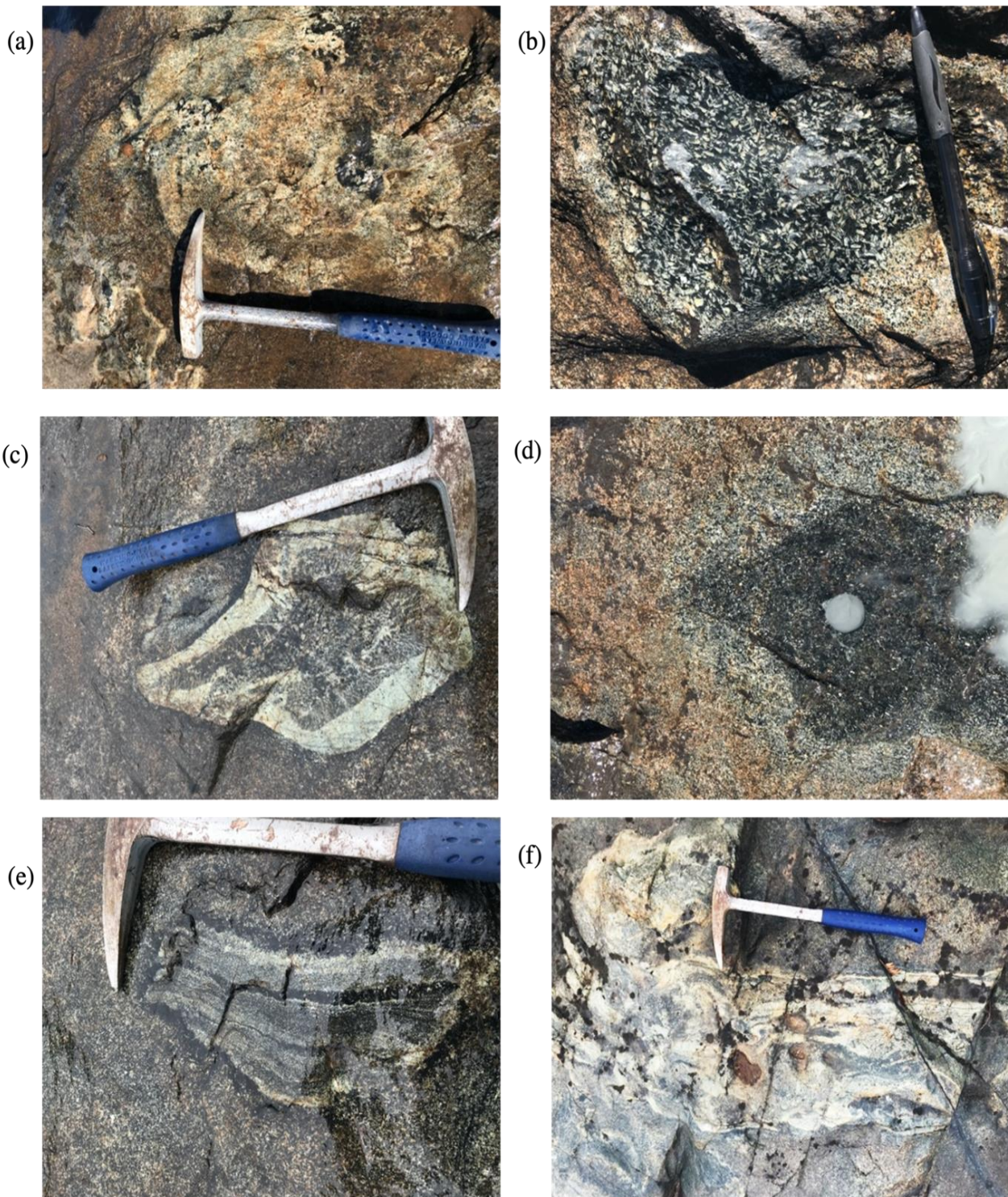


Figure 10 Photographs of the types of xenoliths in the six different categories described above: Figure a) Category A; Figure b) Category B; Figure c) Category C; Figure d) Category D; Figure e) Category E; Figure f) Category F

CHAPTER 3: ANALYTICAL METHODOLOGY AND RESULTS

The proposed research method for this study follows a methodological triangulation (mixed methods) approach in which both quantitative and qualitative research methods are used to meet the research objectives. The quantitative methods used in this study include the geochemical data that were obtained by XRD, XRF, and SEM. The qualitative data in this study include the petrographical analysis of the samples by making thin sections and using microscopy to make physical observations as well as field observations and classifications. The type of mixed methods approach that will be used is the sequential exploratory approach in which qualitative methods are implemented first, and quantitative methods follow afterwards in order to further support the qualitative analysis. Furthermore, this research project can be defined as a case study. This is because the project is based on an in-depth exploration of a particular anomaly that is geographically restricted to a specific location. The project also consists of a small sample size, which enables the research to be concise and specific in its findings. A disadvantage of this would be that the research could be limited in the extent to which the findings can be generalised.

Laboratory techniques

The xenoliths were originally found in one outcrop in the Steelpoort River on the Duikerskrans farm. Further xenoliths were discovered by mapping the rest of the outcrops on an approximately northeast to southwest 2 km traverse along the riverbed. Due to terrain constraints, such as deep water levels and steep banks, sampling of these xenoliths was limited to the outcrops that were most accessible with the handheld core drilling machine. Once the samples were collected and properly labelled, analytical techniques could be employed to analyse the samples. Sixteen core samples were collected that were between 5

and 10 cm in length with a diameter of 3 cm. Of these 16 samples, only eight were chosen for analysis. These were the following samples: AA-01, AA-06, AA-09, AA-10A, AA-10B, AA-11B, AA-11C, and AA-12. Samples that properly intersected the xenolith material, were not extensively weathered, did not contain many cracks, and were mostly intact were selected. Sample AA-01 was a sample of the magnetite gabbro host rock, and the rest of the samples were taken from a variety of different xenolithic bodies.

For the eight samples chosen, polished thin sections were made in the geoscience laboratory at the University of Witwatersrand. These thin sections were used for both petrographic and geochemical analysis with a scanning electron microscope (SEM). The remaining material from each sample was used to obtain X-ray fluorescence (XRF) and X-ray diffraction (XRD) results.

For petrographic analysis, a Leica cross-polarised microscope with a mounted camera was used at the University of Pretoria. The textures described in each sample were observed and high-resolution photomicrographs were taken in cross-polarised as well as plane-polarised light at 5× magnification.

The mineral identification of these samples was obtained using XRD. Samples were analysed using a PANalytical X'Pert Pro powder diffractometer in θ - θ configuration - with an X'Celerator detector and variable divergence and fixed receiving slits with Fe filtered Co-K α radiation ($\lambda=1.789\text{\AA}$). Mineralogy was determined by selecting the best-fit pattern from the ICSD database to the measured diffraction pattern, using the X'Pert Highscore plus software. The samples were prepared by first grinding all samples into a fine powder. For X-ray diffraction analysis, the samples are then pressed as densely as possible into a zero diffraction plate and placed into the XRD instrument. An X-ray beam is then directed at the

sample and the scattered intensity is measured. The measured diffraction pattern will then indicate the sample's crystalline structure, and the phases that are present can be identified.

The major element concentrations for all bulk rock samples were obtained from crushed and powdered samples using the Thermo Fisher ARL Perform X Sequential XRF instrument, and Uniquant software was used for the analyses at the University of Pretoria. These samples are prepped by first baking the powders to remove all volatiles, then adding a flux powder to the samples and melting them down to form fused beads. These fused beads are then placed into the XRF analyser, which will then determine the chemical composition of a sample by measuring the secondary X-ray emitted from a sample when it is bombarded by a primary X-ray beam.

The major element compositions for ilmenite, magnetite, plagioclase, pyroxene, and hornblende were taken with the Zeiss Ultra/X-Beam FEGSEM scanning electron microscope at the University of Pretoria and analysed using AZtec software. Energy dispersive spectroscopy (EDS) points were used, or in some cases, EDS areas were obtained for large homogeneous minerals to determine the major element mineral compositions. All analyses used an accelerating voltage of 15Kv and a processing time of 30 s. These analyses were used to determine the compositions of the end members and calculate An# and Mg#.

Back-scattered electron (BSD) images as well as energy-dispersive spectroscopy (EDS) maps of the major elements were obtained from three samples. These samples were AA-10B, AA-06, and AA-01. The BSD images were obtained on a Zeiss Crossbeam 540 FIB-SEM instrument at Texas Tech University. The images were obtained with a working distance of 8.4mm, a brightness of 48 (a lower brightness was used for images containing ilmenite) and a contrast of 21.8. The EDS maps of these images were also produced under the same running conditions, and the processing time for each map was 5 min. EDS maps were

made for three sites in each thin section, and the elements that were mapped were the following: Si, Al, Na, Ca, K, Mg, Mn, Ti, Fe, and P.

PETROGRAPHY AND GEOCHEMISTRY

In order to conduct the petrographical analysis, the core samples were cut into polished thin sections by the Wits Geoscience lab. These thin sections could then be analysed with the Leica microscope and camera system in order to view the thin sections under microscope and also take high resolution photomicrographs as seen in Figure 11, Figure 12 and Figure 13. The thin section of the host rock was then compared to those of the xenoliths in order to look for any notable differences in the textures and minerals that were present. The thin sections were viewed under cross polarised (XPL) and plane polarised (PPL) light, as well as under reflected light in order to identify all mineral and opaque phases present. High resolution PPL thin section scans were also made at the Texas Tech University geosciences lab. These thin section scans can be viewed in the appendix and served as guidelines to assist in planning where the element maps were made.

The petrographic analysis was performed by first looking at the thin section of the host rock sample AA-01. The photomicrograph seen in Figure 11 (a) and (b) shows the host rock in PPL and XPL. In XPL the characteristic parallel twinning of plagioclase is clearly visible. Furthermore, the sample also contains interstitial clinopyroxene as well as opaque magnetite. Overall, the plagioclase grains appear to be euhedral and largely undeformed and unaltered. The sample shows slight weathering, also visible in the photomicrograph, possibly as a result of exposure on the riverbed. No other textures indicative of deformation or metamorphism can be observed in the host rock, and the minerals and textures present are to be expected from a magnetite gabbro.

In contrast to the host rock specimen, the other thin sections appeared to have completely different minerals and textures. In all thin sections, the plagioclase that was present seemed to be heavily altered and did not preserve the twinning textures in XPL. The

grains were still euhedral and did not appear to have experienced deformation. A notable observation was that magnetite was not present in almost all of the thin sections, and new minerals, hornblende and chlorite, were extremely abundant. The hornblende or green amphibole is recognisable by its bright green colour and strong blue-green pleochroism in PPL. Blue-green chlorite is also frequently seen in association with green amphibole.

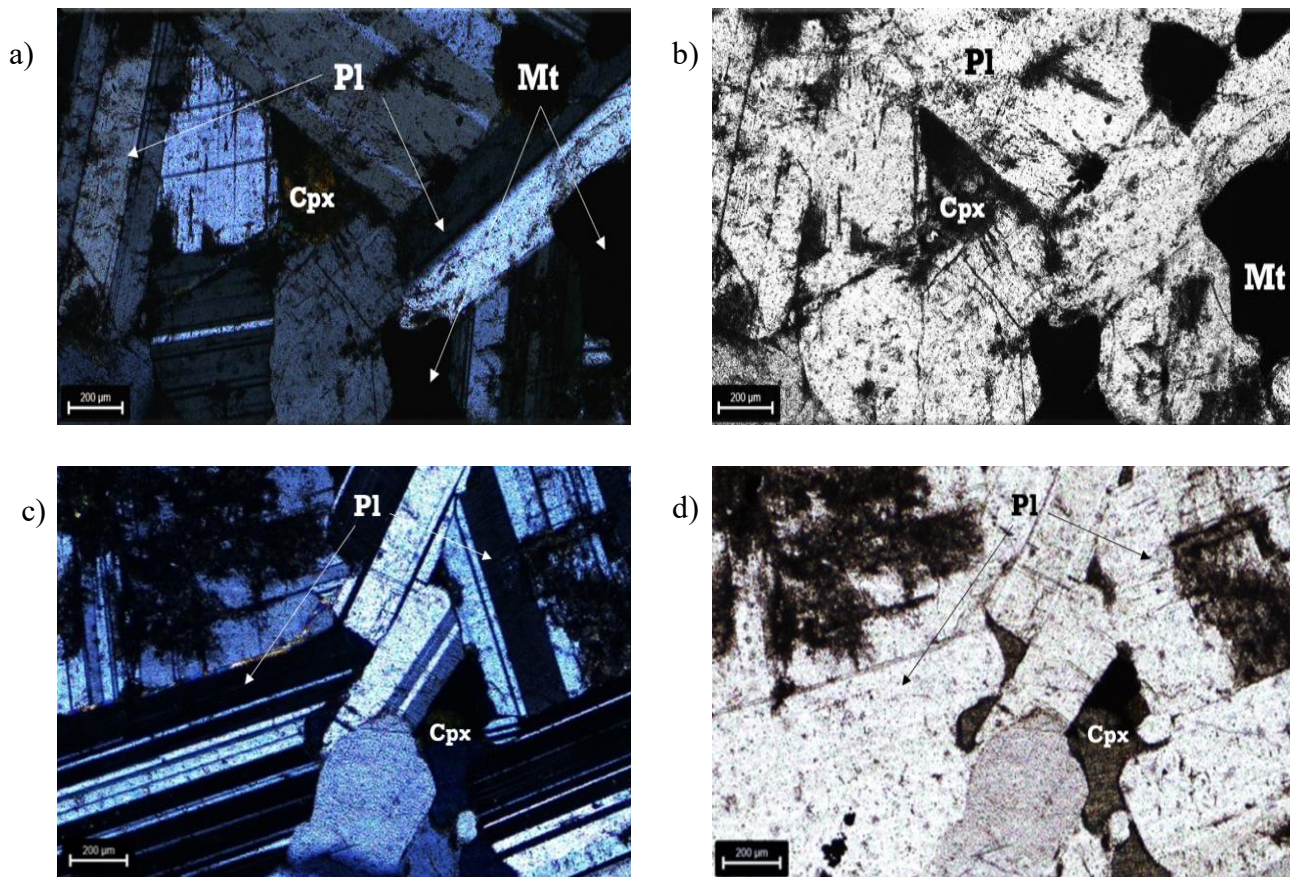


Figure 11 - Photomicrographs taken from the host rock sample showing XPL images in a) & c) and corresponding PPL images in b) and d). In these images mostly unaltered euhedral plagioclase crystals can be seen with minor amounts of interstitial Cpx and the opaque minerals are magnetite.

In Figure 12, several thin sections from different samples are shown. By looking at Figure 12, (c) and (d) of sample AA-09, it appears that the plagioclase grains have undergone possible sericitisation. Figure 12 (c) is in PPL and shows the altered colourless plagioclase

grains. In Figure 12 (d) the sericitisation of the plagioclase grain can be seen in XPL as having higher order birefringence. In Figure 12 (e) and (f), from sample AA-11C, a plagioclase grain is visible that has been fractured and filled with green amphibole. The plagioclase crystals are also overgrown with pleochroic green amphibole.

In Figure 12 (g) and (h), from sample AA-09 and AA-11B, the variety of amphibole textures that are present is shown. In Figure 12 (g) fibrous green amphibole and altered plagioclase is shown in PPL, and in Figure 12 (h) a patchwork texture of amphibole, chlorite, and plagioclase is shown in PPL. In general, the thin sections from the xenolithic samples showed mostly altered plagioclase, interstitial green hornblende, amphibole and chlorite.

A few of the thin sections show a specific lamellar arrangement of opaque minerals are shown in Figure 13 This texture can be described as opaque lamellae parallel to each other and intersecting at 60/120 degrees and is known as a trellis or cloth texture (Von Gruenewaldt et al., 1985). In these thin sections this texture is closely associated with green-brown amphibole, and only appears within the boundaries of amphibole crystals, as seen clearly in Figure 13 (c), (e), (g) and (h). The opaque lamellae were identified as ilmenite due to the lath-shaped crystal structure and weak birefractance, and confirmed using EDS. Therefore, the texture was identified as trellis ilmenite occurring in association with green amphibole. This texture is most clearly visible in samples AA-09, AA-10B and AA-12, although other samples also contain minor occurrences.

Figure 13 (a) and (b) are BSD images of magnetite grains in the host rock sample. Here, we can see the same trellis structure of ilmenite, due to the exsolution of ilmenite from magnetite. This texture has been described previously in UZ rock samples (Von Gruenewaldt et al., 1985) and the trellis exsolution of ilmenite has only been known to occur in magnetite. In Figure 13 (a) and (b), we look at the ilmenite trellis within a magnetite grain. Figure 13 (f)

is the BSD image of Figure 13 (e). Here we can observe the main difference between the textures in the host rock and the textures in the xenoliths. The trellis structures in the xenoliths occur without the presence of magnetite, whereas the host rock shows a normal exsolution of the trellis ilmenite from magnetite. In the BSD images (Figure 13 (f) and (d)) of the xenolith samples, we see the trellis ilmenite structures, but instead of magnetite, amphibole is now present. It is also common to observe bright blue/green chlorite in association with these minerals, as seen on the rim of the grain in Figure 13 (h).

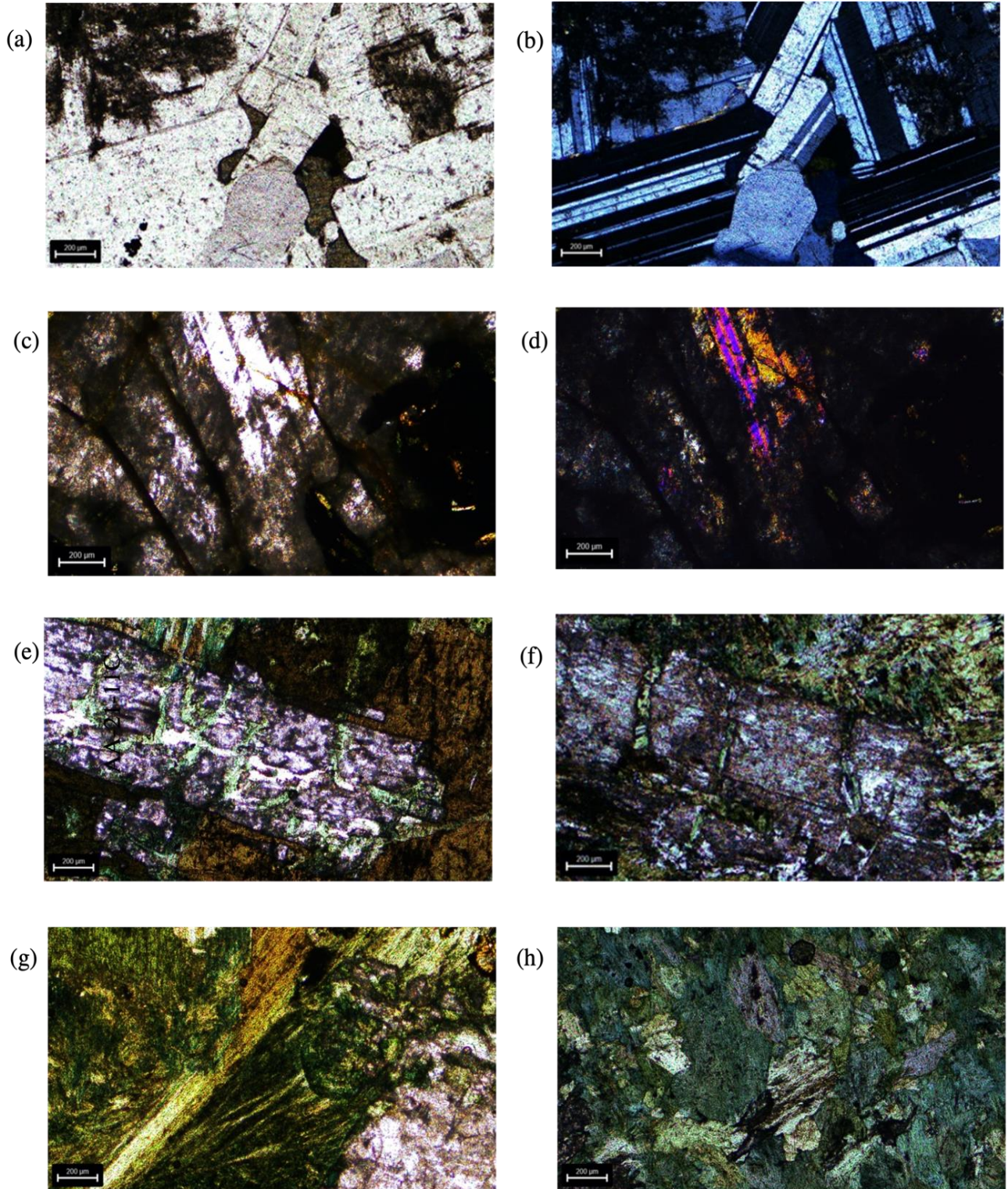


Figure 12- Figures (a) and (b) are PPL and XPL pictures taken in the host rock sample AA-01; Figure (c) and (d) are PPL and XPL pictures taken of sample AA-09 which shows sericitized plagioclase; Figures (e) and (f) are PPL pictures from sample AA-11C showing veins of amphibole crosscutting a plagioclase grain. Figure (g) is a PPL image of sample AA-09 showing fibrous green amphibole; Figure (h) is a PPL image from sample AA-11B showing the large amount of green amphibole and chlorite that is commonly observed.

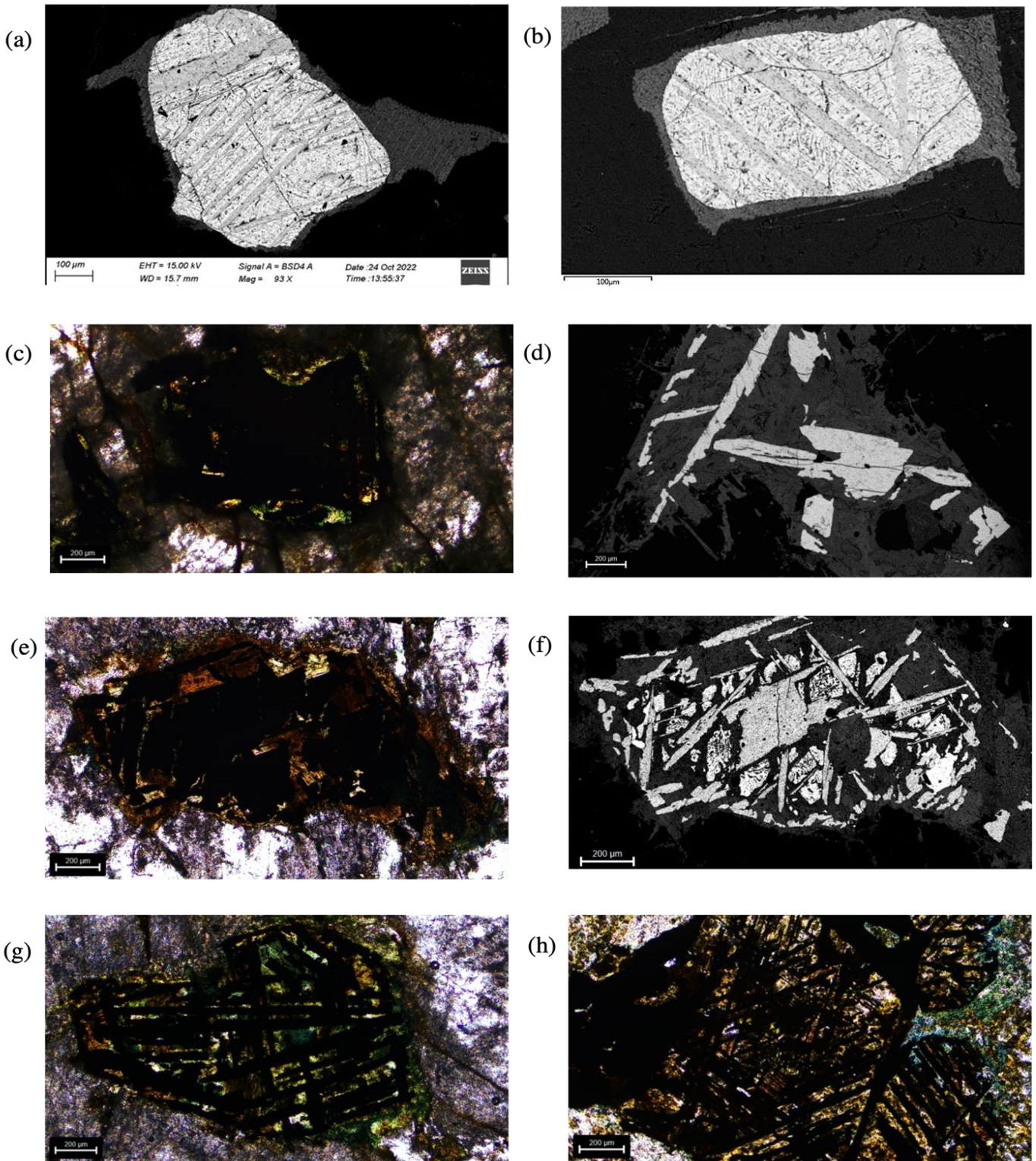


Figure 13- Figures a & b are BSD images showing the normal trellis exsolution of ilmenite within a magnetite grain in sample AA-01, the host rock sample. Figure c, e, g & h are photomicrographs taken in PPL and 5x magnification, showing the remnant ilmenite exsolution and magnetite replaced with hornblende and chlorite from samples AA-09, AA-10B, and AA-12 respectively. Figure d is a BSD image of a remnant ilmenite exsolution with hornblende in sample AA-09. Figure f is the BSD image of figure e.

Geochemistry

The quantitative portion of the data was collected with X-ray fluorescence (XRF), X-ray diffraction (XRD) and scanning electron microscope (SEM) techniques. XRD was used to identify the main mineral phases present in the samples, while XRF was used to obtain the whole rock bulk composition and SEM was used to identify end members and obtain major element oxide compositions of individual minerals in the thin sections.

Table 2 – XRF results showing the major element oxides in each sample. Sample AA-21-01 is the host rock sample, and all other samples are the xenoliths.

	AA - 01	AA - 06	AA - 09	AA - 10A	AA - 10B	AA - 11B	AA - 11C	AA - 12
SiO ₂	46.40	44.76	46.70	50.08	49.55	46.48	45.07	48.13
Al ₂ O ₃	22.24	14.79	17.80	22.19	23.33	18.76	16.12	19.47
MgO	0.52	5.92	3.53	0.34	0.31	3.73	6.28	1.38
Na ₂ O	4.30	1.92	2.85	4.47	4.85	2.93	1.83	3.82
P ₂ O ₅	0.08	0.08	0.03	0.06	0.06	0.11	0.11	0.15
Fe ₂ O ₃	13.01	16.16	14.30	3.63	9.70	12.66	16.05	12.54
K ₂ O	0.60	0.90	0.94	1.24	1.20	1.28	1.18	1.26
CaO	7.48	9.03	8.03	9.87	7.05	8.89	8.71	7.08
TiO ₂	2.20	0.77	1.26	0.07	1.64	0.93	0.52	1.52
V ₂ O ₅	0.03	0.02	0.01	<0,01	0.02	0.01	0.02	0.01
Cr ₂ O ₃	0.01	0.04	0.03	0.01	<0,01	0.02	0.02	0.03
MnO	0.09	0.20	0.20	0.04	0.08	0.16	0.21	0.14
NiO	<0,01	0.01	0.01	<0,01	<0,01	0.01	0.01	0.01
CuO	0.01	<0,01	0.01	<0,01	0.01	<0,01	<0,01	<0,01
ZrO ₂	0.03	0.03	0.02	0.04	0.03	0.02	0.10	0.03
Co ₃ O ₄	0.02	0.02	0.02	0.01	0.02	0.02	0.03	0.02
ZnO	0.01	0.01	0.02	<0,01	0.01	0.01	0.01	0.01
SrO	0.16	0.08	0.11	0.11	0.20	0.12	0.08	0.13
LOI	2.75	5.12	4.05	7.8	1.89	3.78	3.56	4.24
TOTAL	99.94	99.87	99.92	99.95	99.95	99.93	99.92	99.97

Table 3 – XRD results showing mineral phases present within each sample. Sample AA-21-01 is the host rock sample, and all other samples are the xenoliths

	Actinolite	Plagioclase	Prehnite	Chlorite	Ilmenite	Muscovite	Enstatite	Epidote	Dolomite	Magnetite	Augite	Quartz
AA-01	0	87.4	0	1.4	3	2	0	0	0	4.3	2.1	0
AA-06	50.1	31.6	6.8	7.4	0.9	1.1	0	1.5	0.6	0	0	0
AA-09	30.7	42.4	11.5	5.8	3.5	5.4	0	0.2	0.5	0	0	0
AA-10A	9.4	45	32	0.7	0	11.8	1.2	0	0	0	0	0
AA-10B	1.6	72.3	7.6	1.9	2.1	8.3	0	0	0	3.7	2.5	0
AA-11C	47.9	25.2	10.7	9.9	0.1	3.9	2.2	0	0	0	0	0
AA-11B	37.7	36.7	15.2	6.9	1	1.8	0.5	0	0.4	0	0	0
AA-12	23.1	45.6	15.2	2.6	2.2	10.5	0	0	0	0	0	0.8

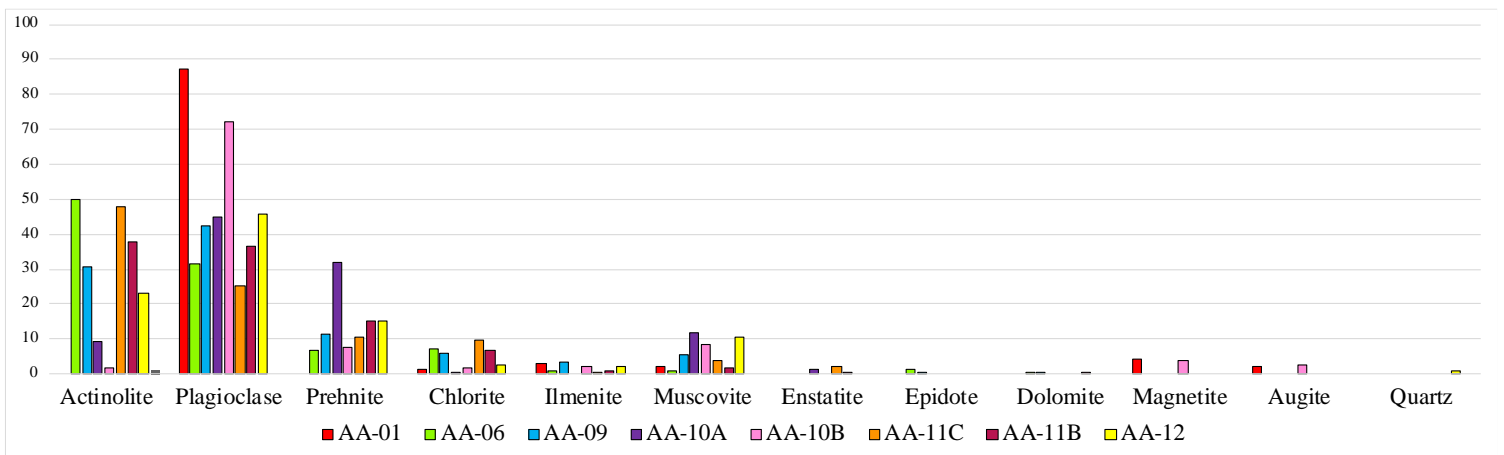


Figure 14 - XRD results visualised as a series of histograms

XRD Results

The XRD results in Table 3 reports the main mineral phases present in each sample as a weight percentage. These results are also visualised in Figure 14 as a series of histograms to indicate which mineral phases are most abundant. As was observed under the microscope, it is confirmed by these results that the host rock, sample AA-01, is mainly made up of plagioclase. The rest of the phases, in order of decreasing magnitude, are magnetite, ilmenite, augite (cpx), muscovite/biotite and chlorite. These are typical phases that one would expect to find in any gabbroic rock. It is now possible to analytically compare how the phases differ from the host rock to the rest of the samples.

The chemical difference between the host rock and the rest of the samples is immediately evident when looking at the results. All of the other samples have a much lower plagioclase content in comparison to the host rock. Sample AA-11C has the least amount of plagioclase (25.2%) and sample AA-10B has the most plagioclase at 72.3%. All of the other samples fall between a range of about 30% to 45% plagioclase, which is significantly lower than the host rock sample. Another big difference is the absence of certain minerals that are present in the host rock, but not in most of the other samples. Magnetite is absent in almost all of the samples, except for sample AA-10B. The same can be said for augite, which is also absent in all of the samples except for sample AA-10B.

Certain phases are not present in the host rock, and only appear in the xenolith samples. Amphibole (noted in the table as actinolite) is the most prominent example of this. The host rock contains no amphibole, yet some of the xenolith samples, like sample AA-06 are made up of 50.1% amphibole. It is important to note that the XRD results cannot distinguish between end members in a mineral series, thus actinolite was identified, but could also represent ferro-actinolite or other orthoamphiboles as well as hornblende. Samples AA-10B and 10A contain the least amount of amphibole, and all other samples fall between the range of 23% and 50%. Another example of this is prehnite, which is present in all samples except the host rock. Sample AA-10A contains the highest amount of prehnite at 32% and sample AA-06 contains the least amount, at only 6.8%.

The behaviour of various other phases could also be observed from these results. Chlorite is present in all samples, but it is notable that the amount of chlorite is higher than the host rock in almost all samples except for sample AA-10A. Similarly, all samples also contain ilmenite as well as muscovite. As stated above, the XRD results cannot distinguish between end members, and thus the muscovite that was identified could also be a different

mineral in the mica group. Most of the samples have more muscovite than the host rock, except for samples AA-11B and AA-06. The ilmenite content of most samples are lower than that of the host rock except for sample AA-09. Enstatite, epidote and dolomite are not present in the host rock, and are only present in samples AA-06, AA-09 and AA-11B. The identification and amounts of phases present in all the samples were valuable in determining the mineral assemblages and illustrating the differences between the host rock and the rest of the samples.

In summary, this data confirms that the xenolith samples contain ilmenite but mostly do not contain magnetite (with the exception of sample AA-10B), whereas the host rock contains both ilmenite and magnetite. Furthermore, we can observe the absence of amphibole (indicated in the table as actinolite) in the host rock, with the xenoliths containing up to 50% amphibole. The xenolith samples also contain prehnite, which is not present in the host rock, as well as higher amounts of chlorite. It should also be noted that the host rock is composed of 87.4% plagioclase, whereas the xenoliths contain only 42.6% plagioclase on average.

XRF Results

The XRF analysis yielded major element geochemical data that was obtained from the whole rock samples. The major element oxide data was then used to plot a series of Harker diagrams as seen in Figure 16 using the computer software R and the GCDkit which enables the user to analyze geochemical datasets. The Harker diagrams were used to compare the ratios of various major element oxide components. For most of the Harker diagrams the variation in MgO content as a weight percentage was plotted on the x-axis and various other oxide elements were plotted on the y-axis. The whole rock bulk composition obtained through XRF was also used to compare to the effective bulk composition which was calculated from EDS element maps.

The major element oxide data from this study was then plotted together with data from other studies in the Upper Zone (Yuan et al., 2017). This was done to compare the geochemistry of these samples to the geochemistry of samples from different subzones in the Upper Zone. The justification for this was that if the major element oxide ratios of these samples are conformable with other Upper Zone samples from the same subzone, they were most likely not foreign to the host rock.

Results obtained from XRF is shown in Table 2 and indicates the weight percentages of all major element oxides present in the samples (the whole rock bulk composition). It was apparent that when plotting MgO against other oxides in Harker diagrams, a trend could be observed in the samples between two ends. Samples AA-10A and AA-10B mostly plotted at one end of this trend, samples AA-11B, AA-09 and AA-12 plotted in the middle, with samples AA-06 and AA-11C plotting at the opposite end. In order to contextualize these results, the data were plotted on Harker plots along with major element oxide data from drill cores sampled at Bierkraal (Yuan et al., 2017).

Bierkraal is located in the western limb of the Bushveld Complex, but if it is assumed that the Bushveld Complex is laterally continuous the lithologies are conformable to the Eastern limb, as seen in Figure 15. There were three drill cores sampled in Bierkraal, visible in the Harker plots below as BK1, BK2 and BK3. BK1 represents Subzone C (UZc) in the lithology, BK2 represents the Upper Main Zone (MZu) and BK3 mostly represents Subzone B (UZb), but also intersects a small portion of Subzone A (UZa). Figure 15 (b) is a simplified stratigraphic column that indicates where the Bierkraal drillcores intersect with the subzones of the UZ.

When comparing the data obtained from the rocks in this study against the data from Bierkraal (Yuan et al., 2017), it can be observed that the rocks in this study mostly overlap with rocks from BK3. BK3 represents UZb and UZa. Both of these subzones are lower in the stratigraphy than UZc, of which the host rock forms part of.

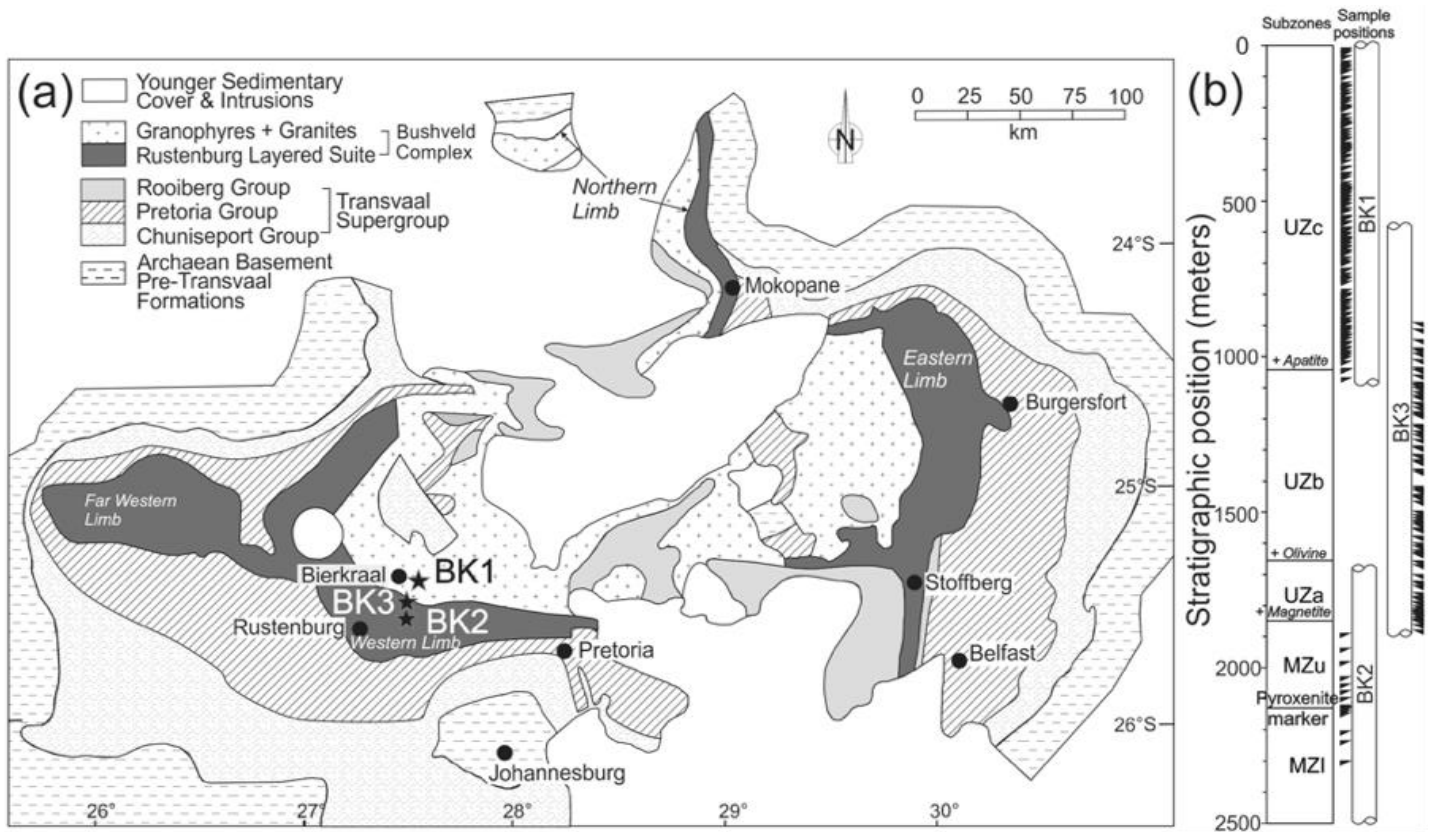


Figure 15 – (a) Geological map indicating the location of BK1, 2 & 3. (b) Simplified stratigraphic column showing where the Bierkraal drill cores intersect the various subzones of the UZ (Yuan, 2017).

SEM/EDS Results

The major element mineral compositions obtained by EDS/SEM was recalculated for each mineral according to (Brady & Perkins, 2023). After the mineral formulae recalculations, each mineral was plotted on its respective ternary diagram, or end-member diagram as can be seen in Figure 17. The amphiboles were classified according to the methodology by (Leake et al., 1997). This process assisted in identifying end-members and comparing variations in minerals found in the host rock with minerals found in the xenoliths. A full table of EDS results and mineral identifications can be found in the additional data spreadsheet.

The mineral major element compositions were used to calculate the plagioclase An content and amphibole Mg# of the samples. As a result of the large variation in An# observed in the xenolith samples, average values could not be plotted. This variation is seen in Figure 17 (a), where An# of xenoliths plot from 100% An to 100% Ab, often in a single sample as is seen in sample AA-09. We also see that many of the xenoliths plot on the alkali feldspar side of the diagram as well, meaning the xenoliths contained plagioclase and K-feldspar. In contrast to this, the An # of the host rock sample is much more consistent and plots in a tight grouping, as indicated by the red shaded area in Figure 17 (a), and has an average An# of 46%.

The ternary diagram for the spinel was plotted by calculating the Ti number ($Ti/(Ti+Fe^{3+}+Fe^{2+})$) and plotting it against the Fe^{3+} number ($Fe^{3+}/(Ti+Fe^{3+}+Fe^{2+})$). This diagram is seen in Figure 17 (b), where the triangles represent magnetite and the circles ilmenite. Ilmenite from all samples is observed to plot relatively close together, with small variations in Ti content. The only two samples containing magnetite were AA-01 and AA-10B. In Figure 17 (b) it is seen that the magnetite of the host rock sample has a higher Ti

content than the AA-10B xenolith sample, and the host rock plots within the titanomagnetite area of the diagram.

The amphibole classification diagram is visible in Figure 17 (c) and was compiled according to the methods in (Leake et al., 1997). It is notable that the amphibole mainly had Mg#s below 0.5, due to a high Fe²⁺ content. The analyses were classified as ferrohornblende, ferrotschermakite, ferroactinolite, and actinolite. The vast majority of amphiboles were

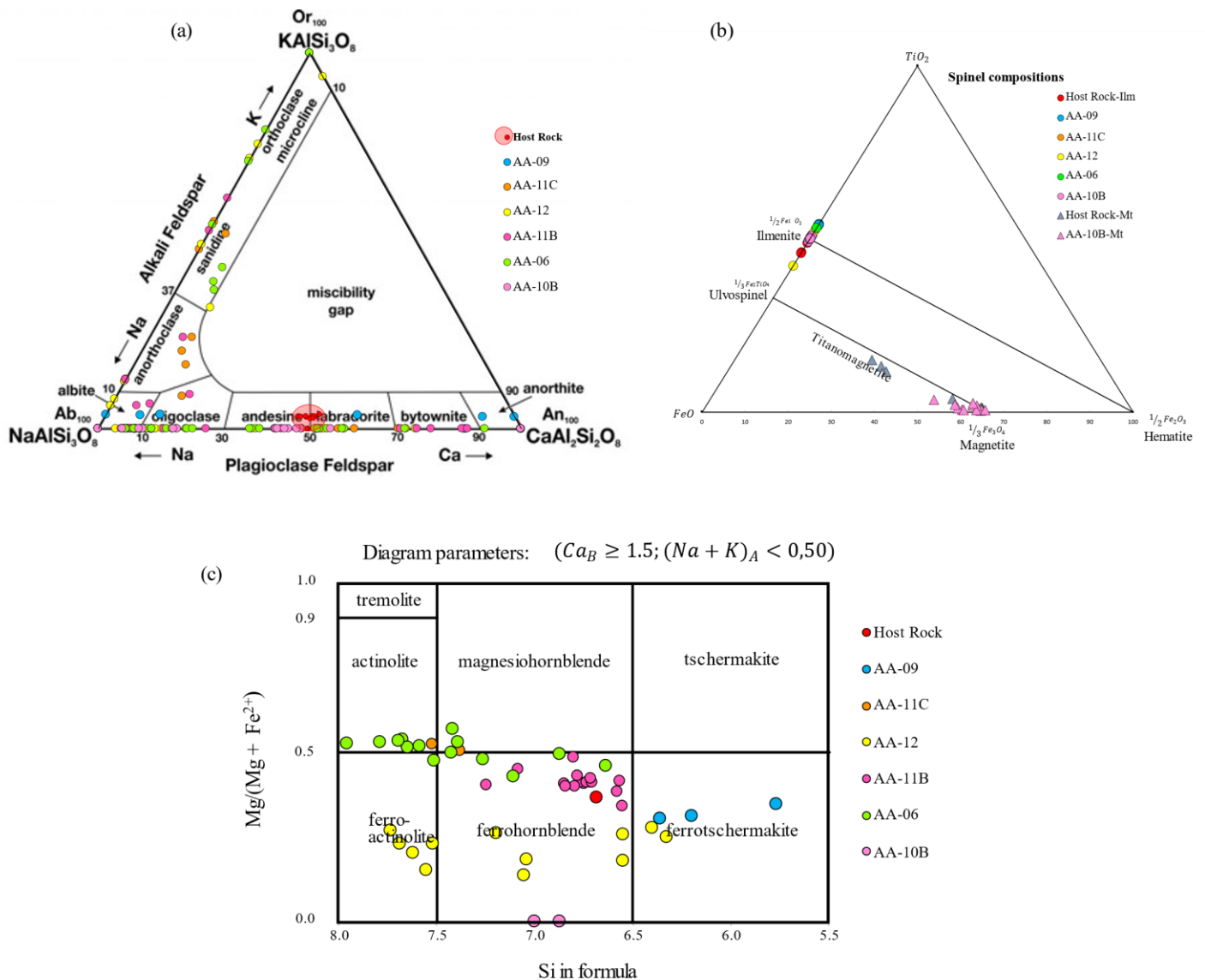


Figure 17 - (a) Ternary diagram of plagioclase, with the host rock sample indicated in the red shaded area. (b) Ternary Spinel diagram indicating ilmenite and magnetite from the host and the xenoliths. (c) Amphibole classification diagram (Leake et al., 1997)

classified as calcic amphiboles, although a small amount of analyses were also classified as sodic-calcic amphiboles and Mg-Fe-Mn-Li amphiboles. In general, the amphiboles were seen to have a high amount of Ca and Fe.

Element maps

Using the SEM instrument at Texas Tech University, maps of major elements could be obtained for three of the samples, and each map would calculate a bulk composition for the selected area. By obtaining an average bulk composition for the maps obtained from each sample, the effective bulk composition (EBC) could be calculated (Sharma et al., 2021). EBC is defined as the closed chemical system that reacts to be in chemical equilibrium (Stüwe, 1997). Initially, these maps were made with the idea of comparing the EBC with the whole rock bulk composition. Three samples were chosen to represent the 'end members' of the system. Sample AA-01 (the host rock) was chosen to represent the least altered sample.

Table 4 - Results obtained from element map effective bulk compositions (EBC) compared to Whole Rock bulk compositions obtained with XRF

	Sample	Site Name	SiO ₂	Al ₂ O ₃	Fe ₂ O ₃	FeO	MgO	TiO ₂	MnO	CaO	Na ₂ O	K ₂ O	SrO	P ₂ O ₅	
Effective Bulk Compositions (EBC) from maps	AA-01	1	58.061	14.701	0	8.6074	0	1.3466	0.0948	11.627	5.2056	0.3568	0	0	
		2	58.824	15.414	0	7.4169	0.5021	1.4357	0	10.825	5.2237	0.358	0	0	
		3	53.2	13.639	0	13.964	1.03	2.8588	0.0975	10.117	4.8001	0.2938	0	0	
		4	54.136	14.483	0	12.787	0.5065	3.1525	0.0959	9.4652	4.9407	0.4334	0	0	
	AA-06	1	53.069	8.3352	0	15.476	7.1345	0.8801	0.2702	11.509	2.7837	0.5427	0	0	
		2	51.44	10.422	0	15.512	6.9129	0.4056	0.0913	11.67	2.9272	0.6191	0	0	
		6	49.735	8.1962	0	15.774	10.21	0.872	0.1785	12.419	2.1451	0.4705	0	0	
	AA-10B	3	59.187	14.948	0	8.7684	0	1.7811	0.0955	8.4555	5.9017	0.8629	0	0	
		4	60.617	14.922	0	7.4965	0.3341	1.0115	0	9.004	5.7569	0.8576	0	0	
		5	63.751	15.527	0	3.8283	0	0.7559	0	9.6896	5.7364	0.7122	0	0	
	Average EBC	AA-01		56.063	14.56	0	10.686	0.5089	2.1952	0.072	10.512	5.043	0.3604	0	0
		AA-06		51.409	8.9754	0	15.588	8.0979	0.7212	0.1804	11.869	2.6158	0.5435	0	0
AA-10B			61.192	15.133	0	6.69	0.1115	1.1811	0.0317	9.0517	5.798	0.8107	0	0	
WR bulk composition (XRF)	AA-01		54.214	15.313	0	12.713	0.911	1.9338	0.0853	9.3642	4.8706	0.4502	0.105	0.0401	
	AA-06		50.432	9.82	0	15.228	9.9438	0.6561	0.1861	10.901	2.0972	0.649	0.0508	0.0359	
	AA-10B		57.388	15.923	0	9.3955	0.5422	1.429	0.076	8.7487	5.4455	0.8865	0.1343	0.031	
EBC - WR bulk composition	AA-01		1.8486	-0.753	0	-2.027	-0.402	0.2614	-0.013	1.1479	0.1725	-0.09	-0.105	-0.04	
	AA-06		0.9767	-0.845	0	0.3608	-1.846	0.0651	-0.006	0.9672	0.5186	-0.105	-0.051	-0.036	
	AA-10B		3.8037	-0.79	0	-2.705	-0.431	-0.248	-0.044	0.303	0.3526	-0.076	-0.134	-0.031	

Sample 06 was chosen to represent the most altered sample (with a grain size small enough to capture a representative bulk composition from the map), and Sample 10B was chosen as a sample between the two extremes. From each sample, approximately three element maps were captured along with their corresponding bulk compositions, and an EBC was calculated from an average of the three maps and compared to the whole rock bulk composition obtained with XRF.

Table 4 shows the results obtained from the calculation of the EBC for each of the maps and compares these values with the whole rock bulk compositions obtained with XRF. It is noted that there is a difference between EBC and WR bulk composition, but the differences were unexpected. Sample AA-10B indicated the largest difference, whereas sample AA-06 and sample AA-01 did not have a significant difference.

Once the element maps were obtained, other interesting observations could also be made. Figure 18 shows the distribution of Ca-rich vs. Ca-poor plagioclase in sample AA-06. Two large plagioclase grains are shown in Figure 18 (a), and the same plagioclase grains can be seen in Figure 18 (b), (c) and (d). Figure 18 (c) is an element map of Ca, and the absence of Ca can clearly be seen in the areas that correspond to the darker grey areas in Figure 18 (a). The plagioclase grain on the right has a zoned appearance, with Ca-poor areas concentrated at the rim. The plagioclase grain on the left, however, is not as neatly zoned and shows a more disseminated texture of Ca-rich and poor areas. The distribution of Ca-rich and Ca-poor zones is also very interesting when comparing the element maps of the host rock to the xenoliths. In the element maps of the host rock, the distribution of Ca in plagioclase is much more uniform. This is to be expected given the EDS results obtained, which are illustrated in Figure 17 (a).

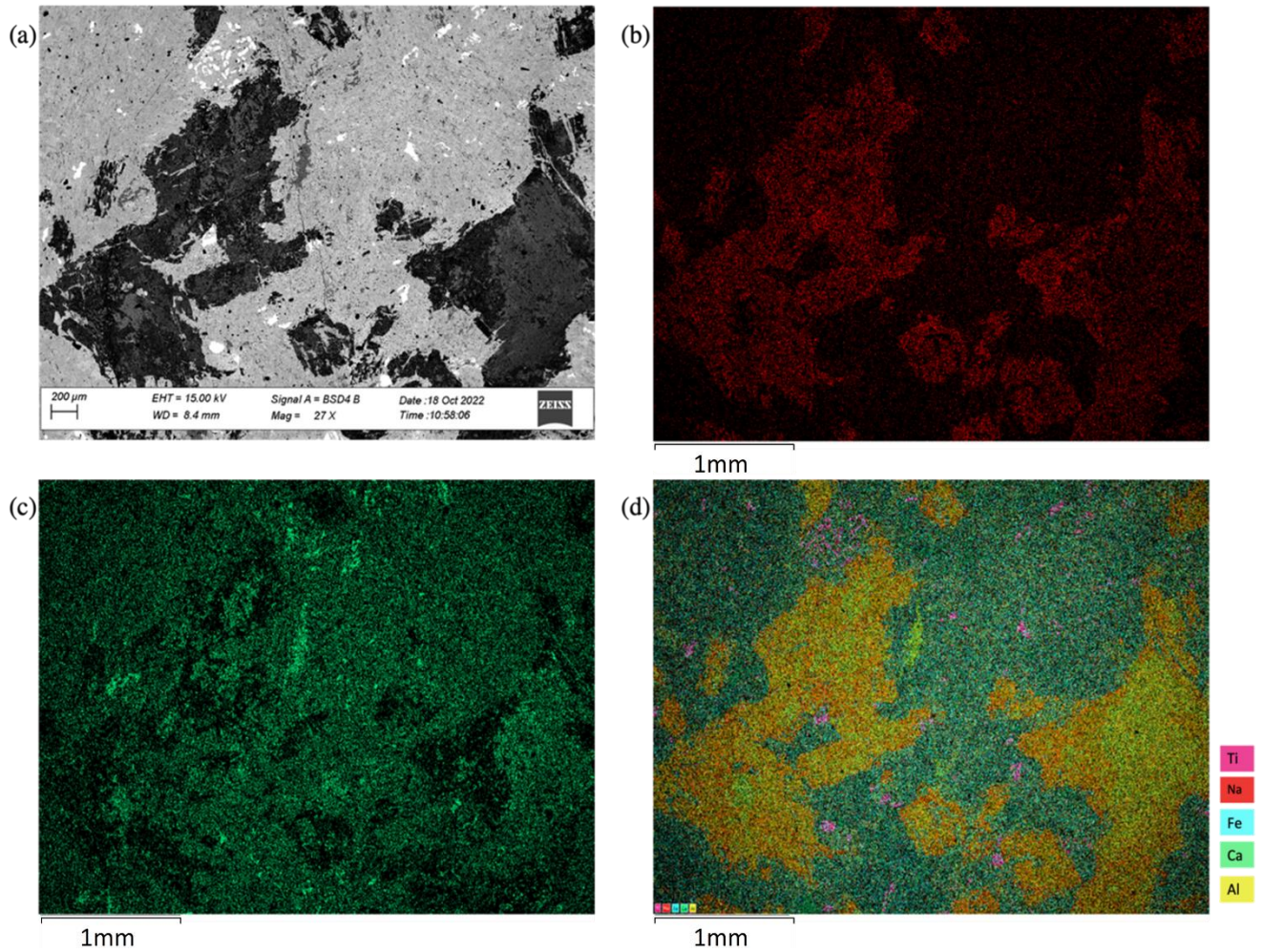


Figure 18 - The distribution of Ca-rich versus Ca-poor plagioclase in sample AA-06 is illustrated using a BSD image (fig (a)), Figure (b) is an element map showing the distribution of Na, figure (c) is an element map showing the distribution of Ca, and figure (d) is a composite element map showing the distribution of Na, Ca, Al, Fe and Ti.

CHAPTER 4: DISCUSSION

The results that have been presented so far can now be used to describe the significance of these findings within the context of the research question and in relation to previous studies in the Upper Zone, in order to answer the research questions:

‘Can the rocks found in the Upper Zone of the Bushveld Igneous Complex in the Roossenekal area be classified as xenoliths?’

and

‘What are the implications of these findings for the emplacement model for the Upper Zone?’

The quantitative and qualitative data can now be analysed and interpreted in order to come to a conclusion.

The geographic spread of the xenoliths

When mapping and categorising the occurrences, the outcrops where the suspected xenoliths were found are plotted on the map in Figure 9. A notable observation that was made was that the vast majority of occurrences were found between outcrops 11 and 7 on the map. Beyond these points, the occurrences were still observed, but there were markedly fewer occurrences per outcrop. A possible explanation for this could be that the occurrences are constrained to a specific layer in the stratigraphy, parallel to the layering of the igneous complex. If this is true, then the natural curves and meanders of the river would not always intersect this layer.

The section of the river that was mapped was roughly parallel to the strike of the complex but began to meander away from this further up and downstream. If the occurrences are confined to a specific layer that is parallel to strike, more of these rocks should be found further along strike, where the river intersects the same layer in the stratigraphy. This is illustrated in Figure

19 where an inferred lineation is illustrated in red. The lateral extent of this layer cannot be inferred and must be investigated further in the field.

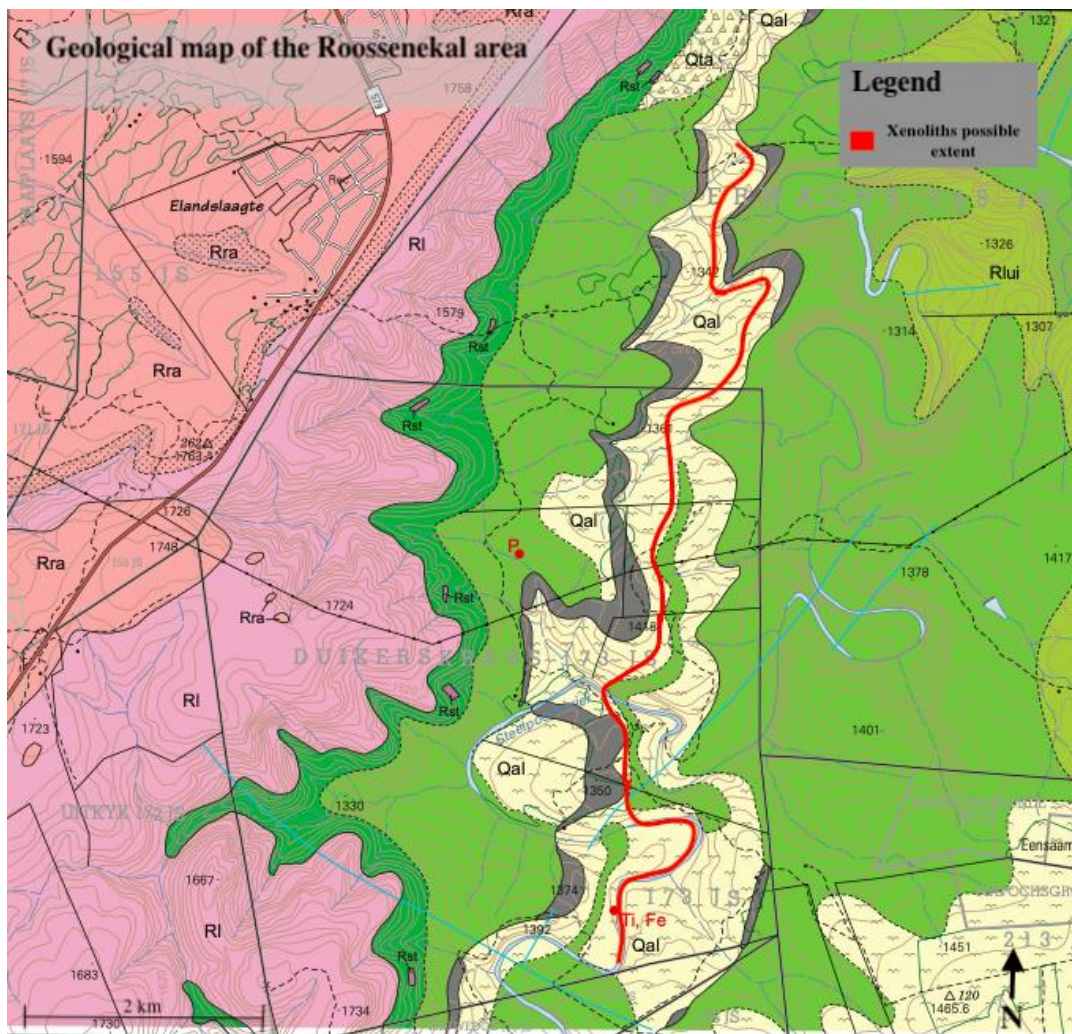


Figure 19 - Map showing the possible extent of the xenoliths (shown in red), if they are confined to a layer in the stratigraphy parallel to strike.

The alteration of plagioclase

The data gathered shows that the samples analysed are mineralogically and texturally different from the host rock. The most notable differences between the host rock and the xenoliths is the alteration of plagioclase in all samples compared to the host rock, the absence of magnetite and augite in almost all samples and the appearance of amphibole, prehnite, and

epidote (not present in the host) in all of the samples. Furthermore, the thin sections revealed green amphibole present in vein-like structures, fracturing some of the plagioclase grains.

There is strong evidence to suggest that all of the samples, excluding the host rock, were subjected to some form of alteration. The plagioclase crystals in all of the samples are heavily altered and do not preserve their lamellar twinning when viewed in XPL, as the host rock does. Another indication of the breakdown of plagioclase can be seen in the XRD results. Prehnite is believed to be produced from the hydrothermal breakdown of plagioclase and is closely associated with sericite (Morad et al., 2010). The sericitisation of plagioclase can be observed in Figure 12 (c) and (d) and was observed in most of the thin sections. This suggests some form of hydrothermal alteration, but it is interesting to note that the same mineralogy was not found in the host rock.

When looking at the EDS results for plagioclase that are illustrated in Figure 17 (a), it is also observed that the xenoliths possess a wide range of plagioclase compositions, whereas the host rock had a much tighter grouping in An#. We can see that in some cases the An# in the xenoliths vary from much as An₁₀₀ (pure anorthite) to An₀ (pure albite) within a single rock. In plagioclase, there exist three miscibility gaps that lead to the formation of distinct intergrowths. These include the peristerite intergrowth (An₂ to An₂₅), the Bøggild intergrowth (An₄₆ to An₆₀), and the Huttenlocher intergrowth (An₆₆ to An₉₀) (Ribbe, 1984). None of the intergrowths in the plagioclase of the xenolith samples fall into one of these classifications. The textures observed in the altered plagioclase crystals can also be seen in the BSD image in Figure 20 below. This type of texture does not resemble the common plagioclase exsolution textures such as Peristerite, Bøggild, or Huttenlocher intergrowths (Ribbe, 1984). Peristerite and Bøggild intergrowths usually have a lamellar appearance, and Huttenlocher intergrowths are a type of spherulitic exsolution that resemble radial clusters. The intergrowths that we

observe in the altered plagioclase of the xenoliths appear to be more disseminated. The distribution of Ca-rich and Ca-poor zones can also be observed Figure 20 and do not show a resemblance to exsolution textures. Therefore, it is concluded that the wide variety of An# together with the disseminated patchwork appearance of the plagioclase would indicate that the textures present are not exsolution textures, but instead alteration textures.

	Spectrum Label	Si	Fe	Ca	Mg	Al	Na	Total
Clinzoisite	Spectrum 337	41.28	4.11	23.96		30.65		100
	Spectrum 338	40.86	4.43	24.42		30.29		100
	Spectrum 339	40.05	4.46	24.57		30.93		100
	Spectrum 349	40.6	4.54	24.06		30.81		100
	Spectrum 352	40.95	4.27	23.54		31.24		100
Plagioclase	Spectrum 335	48.41		25.32		26.27		100
	Spectrum 336	64.78		1.96		22.38	10.88	100
	Spectrum 340	67.47				20.73	11.79	100
	Spectrum 341	46.4		26.6		27		100
	Spectrum 342	67.37				20.81	11.82	100
	Spectrum 345	52.33		18.51		25.81	3.34	100
	Spectrum 346	46.55		26.75		26.69		100

Electron Image 27

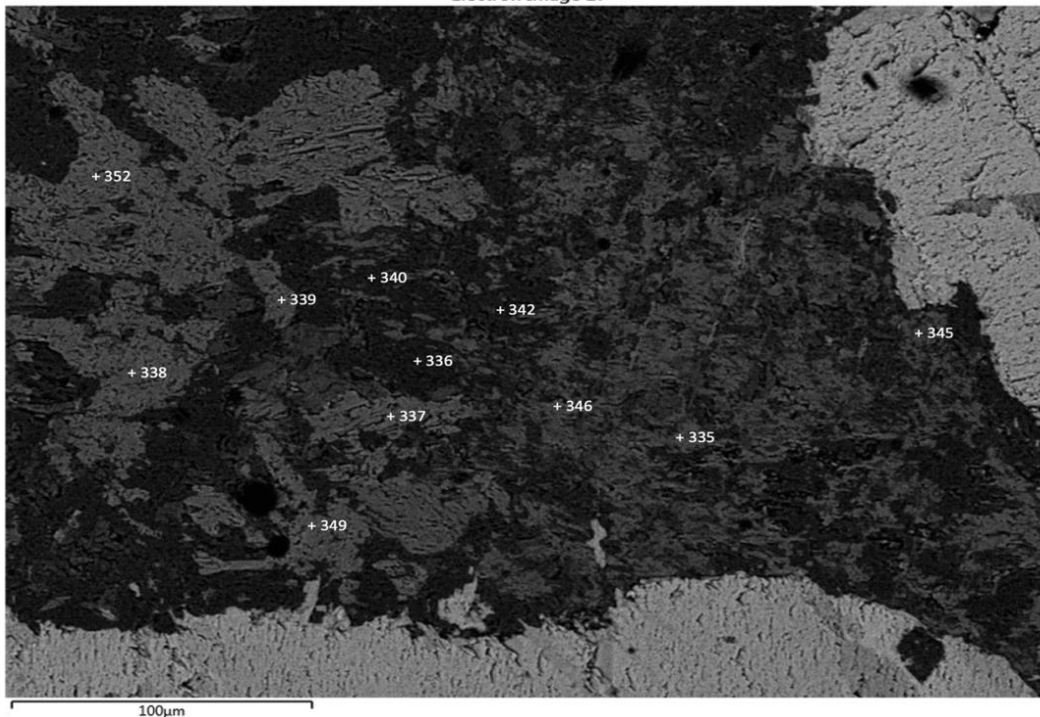
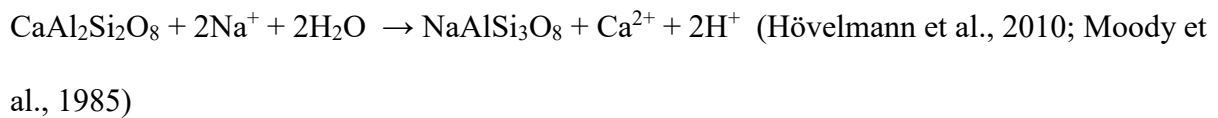


Figure 20 - BSD image from sample AA-11B showing the intergrowth of clinozoisite within an altered plagioclase crystal. The table above is the EDS data showing wt% of element oxides

The evidence suggests that plagioclase crystals have undergone albitization in combination with saussuritization, which are both forms of hydrothermal alteration (Winter, 2013). During albitization, hydrothermal fluids alter plagioclase feldspar to form albite. The circulation of hydrothermal fluids causes a reaction with plagioclase, involving the exchange of Ca and other cations for Na (Hövelmann et al., 2010; Moody et al., 1985). The conversion of plagioclase to albite essentially requires the release of Ca^{2+} and Al^{3+} (Moody et al., 1985). There is more than one chemical equation that can be written to represent the breakdown of plagioclase to albite, however, the reaction can generally be described by the following simplified equation:



In this reaction, Ca in plagioclase is replaced by Na, resulting in the formation of albite. The reaction also produces calcium and hydrogen ions, which can react further with other minerals.

During saussuritization, plagioclase is hydrothermally altered to form an epidote mineral. Unstable Ca-rich plagioclase breaks down to form pure albite, releasing Ca^{2+} and Al^{3+} ions to form an epidote mineral such as clinozoisite (Winter, 2010). These minerals are frequently found in low-grade metamorphic rocks and are known to be the primary reservoir for Ca and Al ions. In a greenschist-facies environment, the expected outcome of plagioclase breakdown is the formation of albite and clinozoisite (Moody et al., 1985). The chemical reaction for this process is:



This provides further evidence that hydrothermal alteration of the xenoliths occurred, as clinozoisite-epidote was frequently observed associated with plagioclase during the SEM analysis. This association can be observed in Figure 20 which is a BSD image of a plagioclase crystal in sample AA-11B. The table above shows the EDS results (wt% oxides) for a number of points within the plagioclase crystal, and here we can clearly see the intergrowth between albite, anorthite, and clinozoisite/epidote.

The disappearance of magnetite

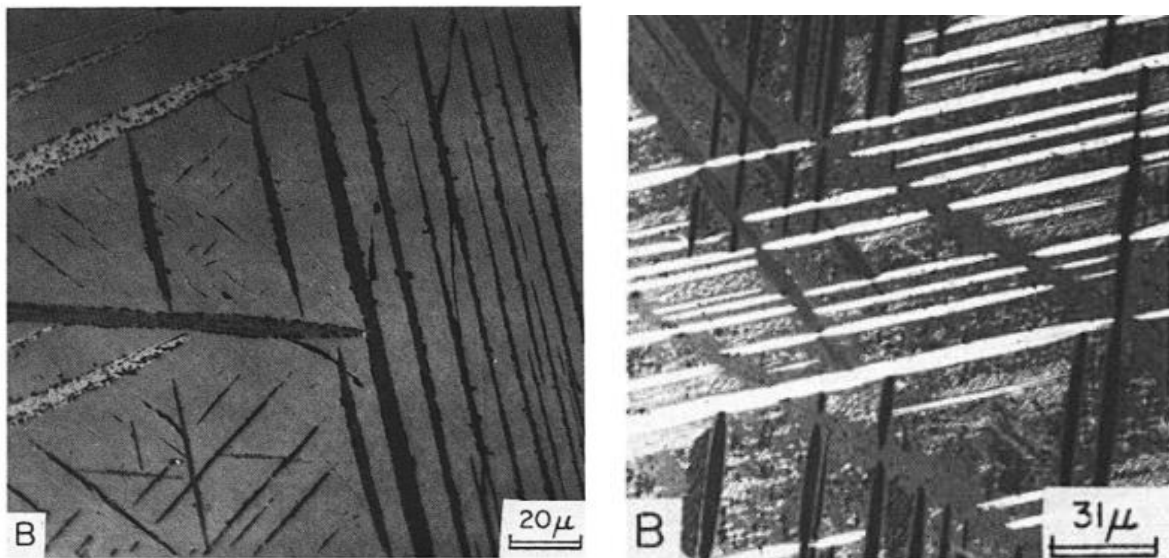


Figure 21 - Trellis exsolution of ilmenite observed in magnetite in the Upper Zone of the Bushveld igneous complex (Von Gruenewaldt et al., 1985)

The absence of magnetite in most of the xenoliths is another significant finding. Magnetite is the most characteristic mineral found in the Upper Zone, which consists of around 25 layers of magnetite hosted in various layers of ferro-gabbro, anorthosite, and norite, which themselves contain fair amounts of magnetite (e.g. Tegner et al. 2006; Yuan et al. 2017). Titanomagnetite in the Upper Zone (both in magnetite layers and in host rocks) is often

associated with the exsolution of ilmenite, as can be seen in Figure 21 (Von Gruenewaldt et al., 1985). The exsolution of ilmenite from magnetite in this case is not a true exsolution, as there is no known solid solution for ilmenite and magnetite (Brzozowski et al., 2021). Instead, ulvöspinel exsolves from the magnetite- ulvöspinel solid solution at temperatures above the magnetite- ulvöspinel solvus and is later oxidised to form ilmenite (Von Gruenewaldt et al., 1985). Another widely accepted theory for the formation of magnetite-ilmenite intergrowths is that the magnetite- ulvöspinel assemblage is oxidized by oxygen rich water in terrestrial environments (Brzozowski et al., 2021) . The exsolution of ulvöspinel will normally occur parallel to the {111} direction and is also called trellis exsolution, as can be observed in Figure 21. Most ilmenite in the titanomagnetite layers probably originated from this oxidation exsolution, although some primary ilmenite does occur in the surrounding mafic units as individual grains (Von Gruenewaldt et al., 1985)

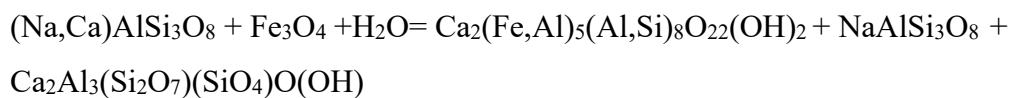
The ilmenite that is present in the xenolith samples closely resembles the trellis exsolution of ilmenite seen in the host rock, but the trellis ilmenite in the xenoliths occurs in the absence of magnetite. Instead of having magnetite, the ilmenite in the xenoliths is surrounded mostly by green amphiboles and chlorite. This leads to the conclusion that the magnetite in the xenolith samples has been completely reacted out and replaced by amphibole leaving behind a relict trellis ilmenite texture. This phenomenon can be seen clearly in the photomicrographs and BSD images in Figure 13 (c) – (h).

The disappearance or replacement of magnetite is a reaction that has not been observed to date in the Upper Zone or the Bushveld Complex, and the mechanism of this reaction is critical to understanding the formation of these xenoliths. In studies associated with porphyry copper deposits, it has been observed that Fe-Ti oxide minerals may experience major compositional and textural changes as a result of hydrothermal alteration (Riveros et

al., 2014). It was also observed that Fe-Ti oxides tend to be destroyed by late-stage acidic fluids associated with the phyllic alteration zone. A similar phenomenon has also previously been observed associated with porphyry copper deposits, where zones of lower magnetic susceptibility were detected with aeromagnetic surveys. These zones were formed due to 'magnetite destructive alteration' caused by the circulation of fluids from an underlying felsic intrusion (Clark & Schmidt, 2001). Considering the fact that hydrothermal alteration is clearly observed in other minerals in the xenoliths, it is plausible that the magnetite in the xenoliths could have been destroyed by magnetite-destructive alteration caused by hydrothermal fluids.

The exact hydrothermal conditions can only be speculated on at this stage until further analysis can be done. From what has been observed thus far it can be concluded that plagioclase and magnetite are reacting hydrothermally to produce albite, epidote/clinozoisite, and amphibole. Based on the conditions under which magnetite-destructive alteration usually occurs, it can be assumed that the alteration was induced by an acidic fluid possibly causing the following generalised reaction to occur:

Plagioclase + magnetite + H₂O = Ca-amphibole + albite + clinozoisite



Considering the range of Ca-amphibole compositions measured in the xenoliths (Figure 17c), it is possible that more than one reaction may have occurred.

Possible origins

The presence of xenoliths in UZc containing magnetite and relict ilmenite would suggest that the source of the xenoliths was a magnetite-bearing unit. The only known magnetite-bearing

rocks in the Bushveld Complex are in the Upper Zone itself, and there are no magnetite-ilmenite bearing rocks reported in the Transvaal Supergroup or surroundings. Therefore, this would imply that the xenoliths originated from the UZ itself, and the xenoliths can be more appropriately classified as autoliths.

The single magma theory for the formation of the Upper Zone suggests that the UZ is the product of the last major melt injection in the Bushveld Complex and differentiated in situ as the result of fractional crystallisation and without the addition of any further magma (Cawthorn & Walraven, 1998; Kinnaird et al., 2002; Kruger, 1990; Kruger, 1994; Kruger, 2005; Tegner et al., 2006; Van Tongeren & Mathez, 2012). The presence of autoliths in UZc would imply two things. First, the autoliths originated from units in the UZ that were fully formed and solidified before UZc was emplaced. Second, this implies that a new pulse of magma was added after the units from which the autoliths originated were formed. This new magma pulse could have been fed through a conduit or feeder dyke (Kruger, 2005) passing through the lower subzones (UZa and UZb), incorporating autoliths from these subzones into the melt and carrying them to higher stratigraphic units where the melt was eventually emplaced, forming UZc. This would effectively disprove the single magma theory, and suggests that there was at least more than one magma pulse in the Upper Zone. Given the information presented so far on the various theories of the formation of the UZ, the existence of autoliths in UZc would be well adapted to the models presented by Scoon and Mitchell, which suggest that several magma pulses are involved in the formation of the UZ.

When analysing the appearance of the different categories of xenoliths, as seen in Figure 10, information about their incorporation into the host magma can be inferred. Certain categories seem to exhibit mostly similar mineralogy, yet have very different physical properties. This can be observed when looking at category B and D which both contain

mostly plagioclase and amphibole, yet category B has a sharp contact with the host rock and category D has a diffuse contact. When xenoliths are incorporated into melt material, assimilation into the host rock can be a relatively slow process. The rate of assimilation depends on the mineralogy of the xenolith and the temperature of the host magma (McLeod et al., 1998). Assimilation may be melt or diffusion dominant, depending on a number of factors, but if the gradual contact with the host rock in category D is a diffusion rim formed during the process of assimilation, then it is evident that category D was in the host magma for a longer period than category B. Similarly, we can infer that the xenoliths with a more deformed appearance, like category F, could have been incorporated into the host magma earlier and subjected to metamorphism for longer, explaining the elongated and deformed shape.

Given that the autoliths have been incorporated into the high temperature magma of UZc, one would expect sanidinite facies metamorphism commonly seen in other xenoliths around the world or other high temperature facies. Instead, the facies of metamorphism that is observed in these autoliths appear to be much lower. With characteristic minerals like chlorite + albite + epidote (or zoisite) + actinolite, the autoliths fit more appropriately into the Greenschist facies or even the sub-Greenschist facies, since minerals like prehnite, pumpellyite, and stilbite (zeolite) have also been observed. One possible explanation for this phenomenon is that the protolith from which the xenoliths came had not fully cooled down by the time the xenoliths were incorporated into the UZc magma. This would cause the temperature difference between the autoliths and the magma to be much smaller. In general, a smaller temperature difference between a xenolith and the host magma could result in less heat transfer and a lower degree of metamorphism. This is because the degree of metamorphism is influenced by factors such as temperature, pressure, and the duration of

interaction between the xenolith and the host magma (O'Sullivan et al., 2021; Winter, 2013; Yamasaki & Uchino, 2023)

The major element geochemistry can be analysed to provide further evidence. When looking at the Harker plots in Figure 16 the major element ratios of the samples in this study are plotted together with data from the Bierkraal drill cores collected from a previous study in the Upper Zone (Yuan et al., 2017). The three different Bierkraal drill cores represent the various different subzones in the Western Limb of the UZ. As can be observed from these diagrams, the major element ratios of the samples in this study seem to overlap to a large extent with samples from the drill core BK3, which mostly represents subzone B and a portion of subzone A. As can be seen in the simplified stratigraphic column in Figure 15, subzone B is lower in the stratigraphy than subzone C of which the host rock forms part. If the samples in this study are assumed to be of an igneous protolith and have geochemistry similar to igneous rocks from subzone B, it is reasonable to assume that these samples are xenoliths that originate from protoliths in subzone B. The problem with this conclusion is that, given other evidence suggesting that the xenoliths have been hydrothermally altered, the bulk composition of the xenoliths could be very different from their original composition or the composition of their protolith.

In open system metasomatism, the chemical composition of a rock is altered by the introduction of chemical components from an external source, such as hydrothermal fluids. This can lead to the addition of new elements to the rock, changing its bulk composition (Winter, 2013). Leaching, a process often associated with hydrothermal alteration, involves the removal of soluble constituents from a rock by fluids. This can result in a loss of mass from the rock, which also alters its bulk composition. The extent of leaching can be assessed through relative or absolute mass changes (Mathieu, 2018). During acid hydrothermal

alteration, large portions of the original rock mass can be effectively replaced by components derived from the percolating acidic fluids. This replacement process can significantly alter the bulk composition of the rock (Darmawan et al., 2022; Winter, 2013). In summary, open system metasomatism and leaching can cause the bulk composition of a rock to change by introducing new elements, removing existing elements, and replacing the original rock mass.

Considering that the xenoliths have been hydrothermally altered and have a bulk composition different from their protolith, it has been much more difficult to constrain the origin of the xenoliths to a specific height in the stratigraphy. For this reason it was decided to compare elements in the xenoliths which were not part of the changing chemical system. Titanium (Ti) was chosen since Ilmenite was the only mineral phase to remain unchanged from the protolith or did not seem to be altered in any way. Aluminium (Al) was also chosen since in general, Al is considered relatively immobile compared to other elements such as Na, Ca, and K during metasomatic processes (Winter, 2013). A graph comparing the Al/Ti ratios of the xenoliths with the Al/Ti ratios of the Bierkraal drillcores was constructed as seen in Figure 22 to try and determine a more precise origin for the xenoliths.

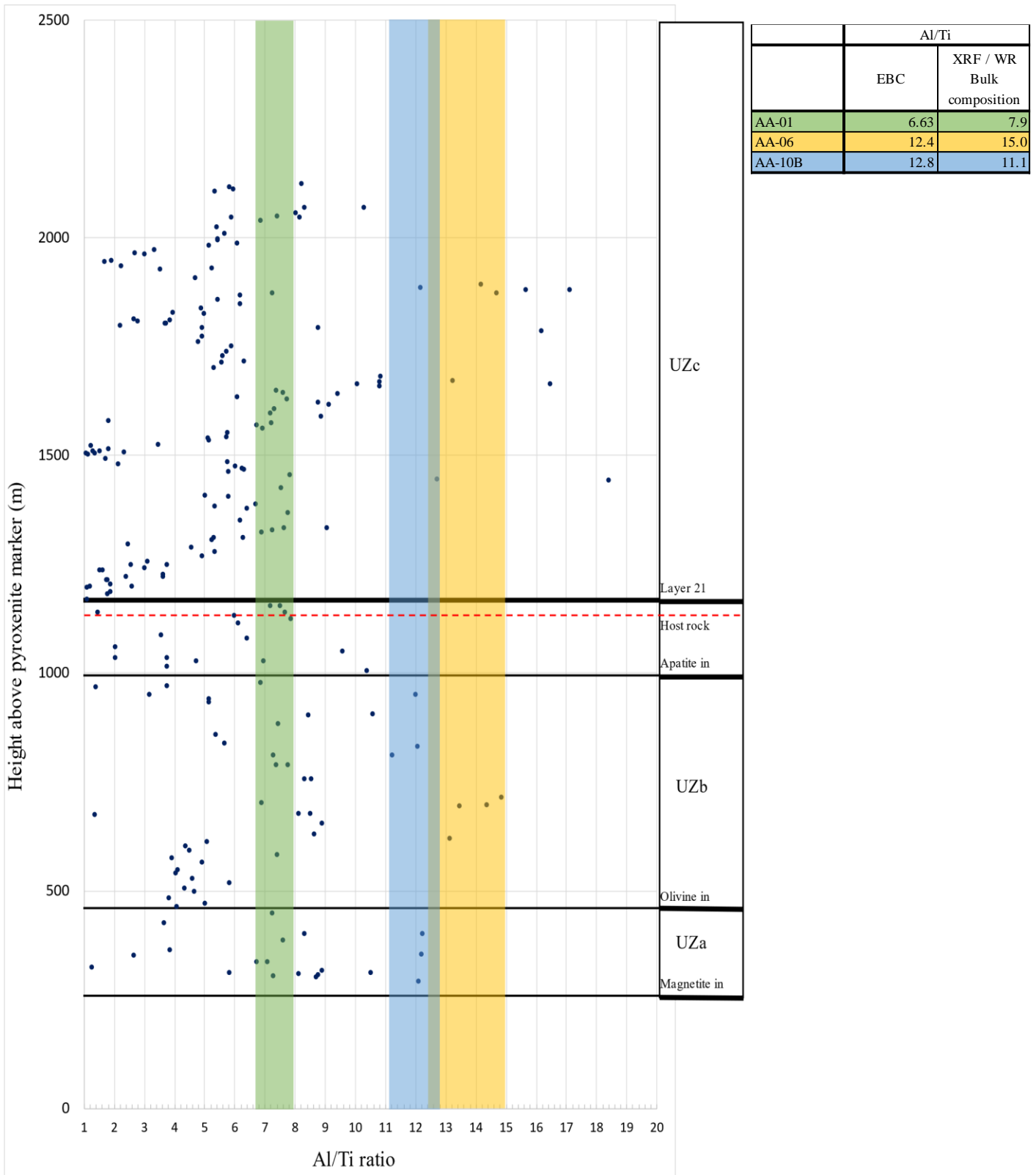


Figure 22 - Al/Ti ratios vs height above the Pyroxenite marker for Bierkraal samples in the Western Limb. Green, Yellow and Blue shaded areas represent the Al/Ti ratio intervals for the xenolith samples AA-01, AA-06 and AA-10B respectively. The dashed red line indicates the position of the host rock in the stratigraphy.

From observing the Al/Ti ratio vs. height profile, it is seen that the green shaded area, which represents the host rock, intersects with matching Al/Ti ratios from the Bierkraal samples at the same height in the stratigraphy. This confirms that the host rock has an Al/Ti ratio that matches the ratio expected for its position in the stratigraphy. The yellow and blue shaded areas representing samples AA-06 and AA-10B do not intersect matching Al/Ti ratios from the Bierkraal samples at their given position in the stratigraphy. When looking at the graph, it is seen that the yellow and blue shaded areas intersect Al/Ti ratios corresponding to much lower positions in the stratigraphy, as well as higher positions. This could give a more accurate representation of the origin of the xenoliths. The lower position would indicate that the xenoliths could have a protolith in UZb and UZa and were possibly transported upwards via conduits to UZc. The higher position is less likely to be the possible origin, since this would indicate that the xenoliths had a protolith in an upper part of UZc. For this to be possible we would have to consider a non-sequential emplacement model, meaning that the upper portion of UZc was emplaced before the lower portion, and the xenoliths fell into the lower portion when it was injected as a sill-like structure at a later stage. Such an out-of-sequence emplacement model has previously been suggested for the Lower and Critical Zones (Mungall et al., 2016; Yao et al., 2021) but has not been previously considered for the Upper Zone.

Another factor to consider when comparing Al/Ti ratios in the xenoliths is the fact that there might have been at least some degree of movement of Al within the system. This is considered since plagioclase is the main source of Al in the system and has also been extensively altered as shown above. If this is the case then Al might not be a good baseline element with which to compare the xenoliths to the host rock. In Figure 23 box and whisker

plots are shown for Al content in plagioclase crystals from all the samples. From this it is apparent that there is a much higher degree of variance in the xenolith samples compared to the host rock (AA-01). This is because there could possibly have been movement of Al from plagioclase out of the xenoliths through hydrothermal fluids. Alternatively, Al could also have remained in the xenoliths and the main sink for Al would be amphibole. If this is the case the bulk Al in the samples would not be greatly different from their protolith and Al would still be a useful indicator element. Despite some uncertainties regarding the mobile elements and chemical alteration of the system, it is still noteworthy that in both methodologies that were applied to identify a protolith for the xenoliths, Subzones A and B were concluded to be viable options.

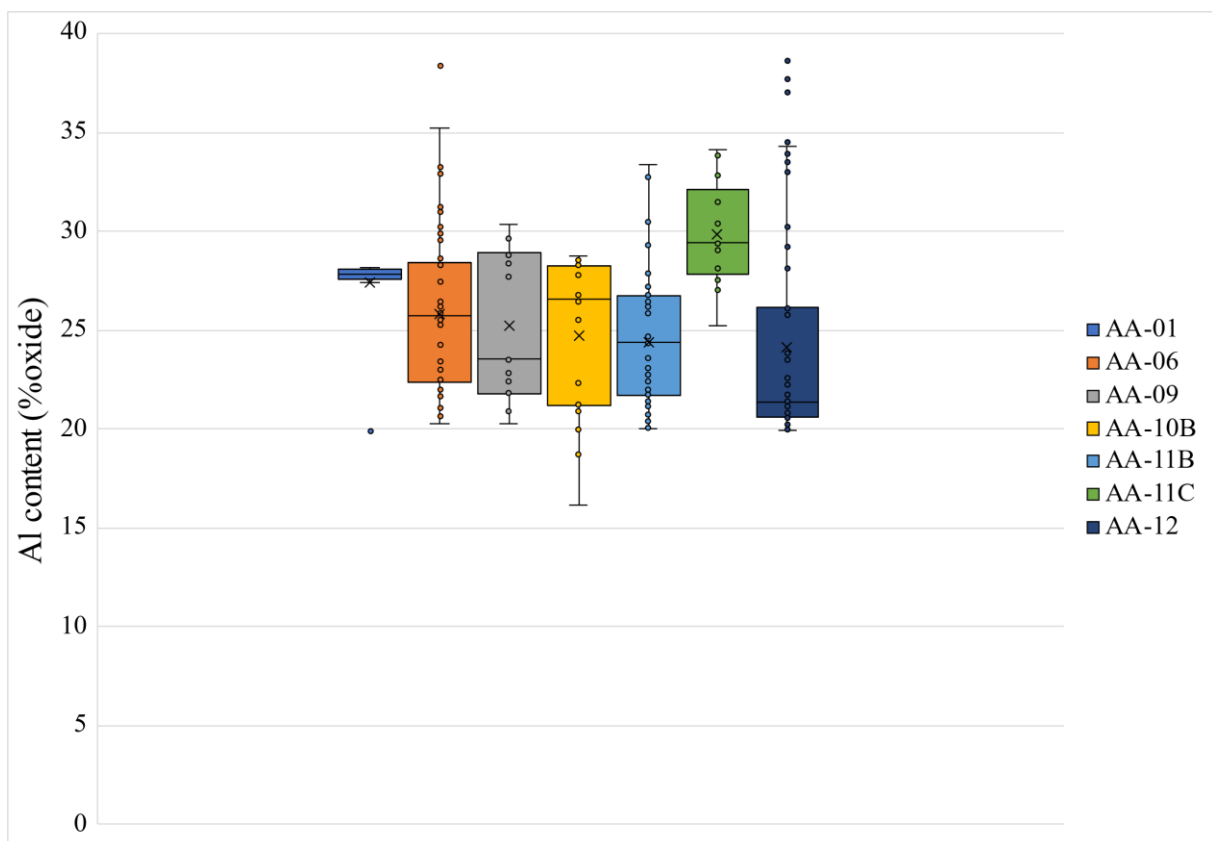


Figure 23 - Box and Whisker plot comparing the Al content of plagioclase crystals in weight% oxides between all samples. It is seen that Al content varies greatly in plagioclase crystals from the xenolith samples, but the host rock (AA-01) has much less variance.

The implications of these findings are significant when reviewing the data in the context of previous research. The most widely accepted theory for the formation of the Upper Zone is the single magma theory, which suggests that the Upper Zone is the product of the last major melt injection in the Bushveld Complex and differentiated in situ as the result of fractional crystallization and without the addition of any further magma (Cawthorn & Walraven, 1998; Kinnaird et al., 2002; Kruger, 1990, 1994, 2004; Tegner et al., 2006; Van Tongeren & Mathez, 2012). The presence of autoliths formed from UZa or UZb protoliths would imply two things. Firstly, subzones B and A were fully formed and solidified before subzone C was emplaced. Secondly, this implies that a new pulse of magma must have been added after subzones B and A were formed. This new magma pulse could have been fed through a conduit passing through subzones B and A, incorporating xenoliths from these subzones into the melt and carrying them to higher levels where the melt was eventually emplaced forming subzone C. This would effectively disprove the single magma theory, and suggests that there was at least more than one magma pulse in the Upper Zone.

Limitations and recommendations

Certain aspects of this project could not be addressed due to limitations in time and resources. A large number of possible xenoliths observed in the field fell into categories E and F, as seen in Figure 10. These xenoliths are believed to be of sedimentary origin, unlike the xenoliths that have been discussed in geochemical and petrographic analysis, which were of igneous origin. These sedimentary xenoliths have been sampled, but have not yet been analysed in order to identify their mineralogy and geochemistry. This was due to time and resource restrictions, but does not take away from the validity of the results from the other samples. This is because the origin and presence of sedimentary xenoliths in host rock can potentially

warrant a study in its own right. Suggestions for further research regarding this would be to obtain more samples from these categories, make thin sections for petrographic analysis, and perform XRD and XRF analysis on these samples to try and determine a possible protolith. The existence of sedimentary xenoliths and igneous xenoliths in the same host rock should be explored further in order to understand how they came to be hosted within the same magma.

Further research to be done on this project includes more laboratory analysis, as mentioned above, more field work, as well as the modelling of pressure and temperature conditions using thermodynamic software analysis. The geochemical analysis of samples in this study should be expanded to include trace element and isotopic data that can be combined with the major element geochemistry to strengthen the findings in this paper. Furthermore, the study would require more field work to investigate the full extent of this occurrence. This can be done by trying to find more of these outcrops in the suggested area indicated in red in Figure 19. If more occurrences are found, more samples can be taken and analysed to compare with the data thus far. Lastly, the metamorphic and igneous conditions that formed these xenoliths can be modelled with thermodynamic software by using the phases that are present as well as bulk rock compositions to understand their petrogenesis more completely.

This research could also greatly benefit from a fluid inclusion study and a more in-depth analysis of the amphibole in the xenoliths to determine the nature of the hydrothermal fluids responsible for the metamorphism. This would help to understand the hydrothermal reaction of plagioclase with magnetite, which is not yet well understood. For calculating the EBC it is also recommended that element maps be produced for the entire thin section instead of only 3 maps per thin section. This would help to calculate a more accurate EBC as suggested by the methodology of (Sharma et al., 2021). Future research should continue to investigate the nature and origin of these xenoliths, as well as the implications of their presence on our understanding of the Bushveld Complex's formation and evolution.

CHAPTER 5: CONCLUSION

When regarding all the evidence brought forward thus far, the primary research question can be answered. It can be said with a relative degree of certainty that the rocks that have been investigated in this study are indeed xenoliths of an igneous origin. The mineral phases that have been identified by petrographic and XRD analysis confirm the presence of metamorphic minerals like amphibole, prehnite and epidote which are not present in the host rock. Evidence of alteration and metamorphic reactions were also observed in the thin sections of these samples and was not observed in the host rock. The presence of relict trellis ilmenite in the absence of magnetite is perhaps the most significant finding, given that these textures have not been properly described before. The conclusion that the xenolith samples originally contained magnetite also solidifies the idea that these xenoliths had a protolith in the Upper Zone since the Upper Zone is the only magnetite bearing unit in the Bushveld Complex. This idea is further supported when analysing the major element geochemistry and bulk rock compositions of the samples. The major element geochemistry of the xenoliths were markedly different to that of the host rock, and when compared to samples taken from other subzones in the Upper Zone were found to overlap to a high degree with samples from subzones B and A.

This finding led to the answer of the secondary research question, which considered the implication of this study on the model of emplacement of Upper Zone magmas. The existence of xenoliths in subzone C that were derived from intrusions formed earlier in the history of the Upper Zone has major implications on models that have been presented thus far. Previous research indicates that the isotopic homogeneity of the Upper Zone is an indication that the Upper Zone was formed through closed system fractionation of a single magma chamber that did not experience the addition of any new magma pulses. Alternative theories have postulated that the Upper Zone could have possibly experienced more than one magma

pulse due to the presence of mineral reversals in the stratigraphy, and the xenoliths that were found in the Roossenekal area are the physical evidence to support that theory. The presence of xenoliths in subzone C, that have a protolith elsewhere in the Upper Zone would imply that those units must have been fully formed and solidified before the emplacement of subzone C. This also implies that after the formation of the protolith of the xenoliths, a new magma pulse could have been fed through a conduit intersecting the lower subzones of the Upper Zone and incorporating material from these units into the host magma, transporting them to higher units where subzone C would be emplaced.

Moreover, the presence of xenoliths displaying greenschist or sub-greenschist facies metamorphism, which indicates a lower temperature difference with the host magma, adds another layer of complexity to our understanding of the Bushveld Complex's formation. This finding highlights the need for further research into the thermal history and metamorphic processes that have shaped this unique geological feature.

In summary, the discovery of xenoliths in the eastern Bushveld Complex has opened new avenues for understanding the formation and evolution of this massive geological structure. The presence of these xenoliths, their unique mineral textures, and evidence of hydrothermal alteration challenge existing theories and call for further research to unravel the complex history of the Bushveld Complex. As our understanding of this geological phenomenon grows, so too will our ability to harness its economic potential and appreciate the intricate processes that have shaped our planet's geology.

BIBLIOGRAPHY

- Ashwal, L. D., Webb, S. J., & Knoper, M. W. (2005). Magmatic stratigraphy in the Bushveld Northern Lobe; Continuous geophysical and mineralogical data from the 2950 m Bellevue drillcore. *South African Journal of Geology*, 108(2), 199-232.
- Boshoff, J. C. (1942). The upper zone of the Bushveld complex at Tauteshoogte (Dissertation, University of Pretoria, Pretoria, South Africa).
- Brady, J., & Perkins, D. (2023, October 18,). Mineral Formulae Recalculation. SERC. Retrieved April, 2021, from <https://serc.carleton.edu/18592>
- Brzozowski, M. J., Samson, I. M., Gagnon, J. E., Linnen, R. L., & Good, D. J. (2021). Effects of fluid-induced oxidation on the composition of Fe–Ti oxides in the Eastern Gabbro, Coldwell Complex, Canada: implications for the application of Fe–Ti oxides to petrogenesis and mineral exploration. *Mineralium Deposita*, 56(3), 601-618.
- Cawthorn, R. G., & Walraven, F. (1998). Emplacement and Crystallization Time for the Bushveld Complex. *Journal of Petrology*, 39(9), 1669-1687.
- Clark, D. A., & Schmidt, P. W. (2001). Petrophysical properties of the Goonumbla Volcanic Complex, NSW: Implications for magnetic and gravity signatures of porphyry Cu-Au mineralisation. *Exploration Geophysics (Melbourne)*, 32(4), 171-175.
- Darmawan, H., Troll, V. R., Walter, T. R., Deegan, F. M., Geiger, H., Heap, M. J., Seraphine, N., Harris, C., Humaida, H., & Müller, D. (2022). Hidden mechanical weaknesses within lava domes provided by buried high-porosity hydrothermal alteration zones. *Scientific Reports*, 12(1), 3202.
- Eales, H. V., & Cawthorn, R. G. (1996). The Bushveld Complex. *Developments in Petrology*, 15, 181-229.
- Eriksson, P. G., Hattingh, P. J., & Altermann, W. (1995). An overview of the geology of the Transvaal Sequence and Bushveld Complex, South Africa. *Mineralium Deposita*, 30, 98-111.
- Hövelmann, J., Putnis, A., Geisler, T., Schmidt, B. C., & Golla-Schindler, U. (2010). The replacement of plagioclase feldspars by albite: observations from hydrothermal experiments. *Contributions to Mineralogy and Petrology*, 159(1), 43-59.
- Irvine, T. N., Keith, D. W., & Todd, S. G. (1983). The JM platinum-palladium reef of the Stillwater Complex, Montana; II, Origin by double-diffusive convective magma mixing and implications for the Bushveld Complex. *Economic Geology*, 78(7), 1287-1334.


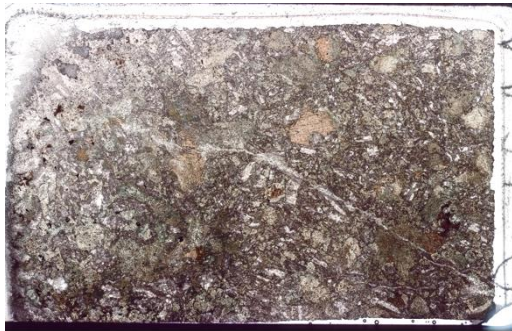

- Kinnaird, J. A., Hutchinson, D., Schurmann, L., Nex, P. A. M., & de Lange, R. (2005). Petrology and mineralisation of the southern Platreef: northern limb of the Bushveld Complex, South Africa. *Mineralium Deposita*, 40(5), 576-597.
- Kinnaird, J. A., Kruger, F. J., Nex, P. A. M., & Cawthorn, R. G. (2002). 4. Bushveld Complex and other intrusions. *Economic Geology Research Unit, Information Circular*, (362), 57-62.
- Kruger, F. J., & Smart, R. (1987). Diffusion of trace elements during bottom crystallization of double-diffusive convection systems: the magnetite layers of the Bushveld Complex. *Journal of Volcanology and Geothermal Research*, 34(1-2), 133-142.
- Kruger, F. J. (1990). The stratigraphy of the Bushveld Complex: a reappraisal and the relocation of the Main Zone boundaries. *South African Journal of Geology*, 93(2), 376-381.
- Kruger, F. J. (1994). The Sr-isotopic stratigraphy of the western Bushveld Complex. *South African Journal of Geology*, 97(4), 393-398.
- Kruger, F. J. (2005). Filling the Bushveld Complex magma chamber: lateral expansion, roof and floor interaction, magmatic unconformities, and the formation of giant chromitite, PGE and Ti-V-magnetite deposits. *Mineralium Deposita*, 40(5), 451-472.
- Leake, B. E., Wooley, A. R., Arps, C. E. S., Birch, W. D., Gilbert, M. C., Grice, J. D., Hawthorne, F. C., Kato, A., Kisch, H. J., Krivovichev, V. G., Linthout, K., Laird, J., Mandarino, J., Maresch, W. V., Nickel, E. H., Rock, N. M. S., Schumacher, J. C., Smith, D. C., Stephenson, N. C. N., . . . Youzhi, G. (1997). Nomenclature of amphiboles; report of the Subcommittee on Amphiboles of the International Mineralogical Association Commission on New Minerals and Mineral Names. *European Journal of Mineralogy (Stuttgart)*, 9(3), 623-651.
- Lenhardt, N., & Eriksson, P. G. (2012). Volcanism of the Palaeoproterozoic Bushveld Large Igneous Province: The Rooiberg Group, Kaapvaal Craton, South Africa. *Precambrian Research*, 214-215, 82-94.
- Maier, W. D., Barnes, S. & Groves, D. I. (2013). The Bushveld Complex, South Africa: formation of platinum–palladium, chrome- and vanadium-rich layers via hydrodynamic sorting of a mobilized cumulate slurry in a large, relatively slowly cooling, subsiding magma chamber. *Mineralium Deposita*, 48(1), 1-56.
- Mathieu, L. (2018). Quantifying Hydrothermal Alteration: A Review of Methods. *Geosciences*, 8(7).
- Molyneux, T. G. (1970). The geology of the area in the vicinity of Magnet Heights, Eastern Transvaal, with special reference to the magnetic iron ore. *Geological Society of South Africa Special Publication*, 1, 228-241.

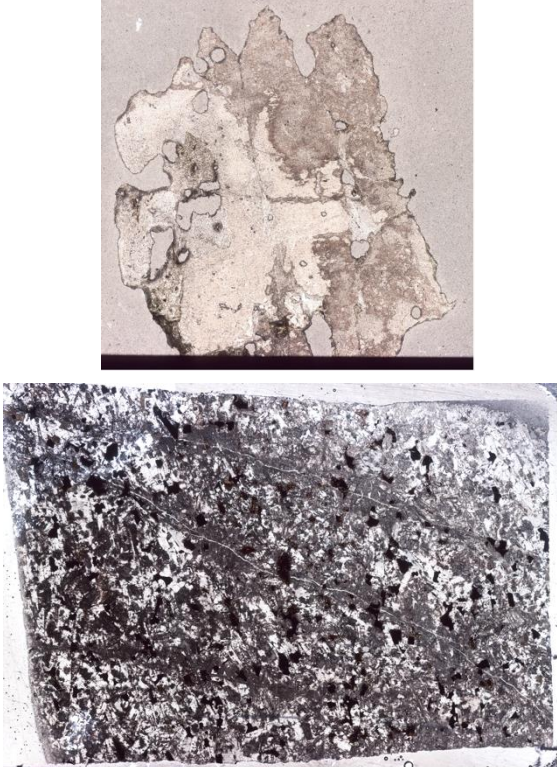
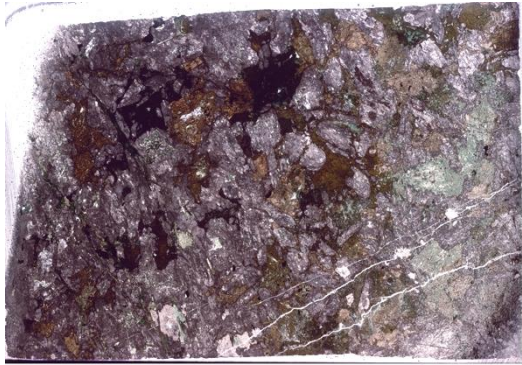
- Moody, J. B., Jenkins, J. E., & Meyer, D. (1985). An experimental investigation of the albitization of plagioclase. *Canadian Mineralogist*, 23, 583-596.
- Mungall, J. E., Kamo, S. L., & McQuade, S. (2016). U–Pb geochronology documents out-of-sequence emplacement of ultramafic layers in the Bushveld Igneous Complex of South Africa. *Nature Communications*, 7(1), 13385.
- O'Sullivan, G. J., Thakurdin, Y., Bolhar, R., Horváth, P., Hoare, B. C., & Collerson, K. D. (2021). The Great Falls Tectonic Zone after the assembly of Laurentia: evidence for long-term tectonic stability from xenolith apatite. *Lithos*, 384-385, 105977.
- Riveros, K., Veloso, E., Campos, E., Menzies, A., & Véliz, W. (2014). Magnetic properties related to hydrothermal alteration processes at the Escondida porphyry copper deposit, northern Chile. *Mineralium Deposita*, 49(6), 693-707.
- Rose, D., Viljoen, F., Knoper, M., & Rajesh, H. (2011). Detailed assessment of platinum-group minerals associated with chromitite stringers in the Merensky Reef of the eastern Bushveld Complex, South Africa. *The Canadian Mineralogist*, 49(6), 1385-1396.
- Scoates, J. S., Wall, C. J., Friedman, R. M., Weis, D., Mathez, E. A., & VanTongeren, J. A. (2021). Dating the Bushveld Complex: Timing of Crystallization, Duration of Magmatism, and Cooling of the World's Largest Layered Intrusion and Related Rocks. *Journal of Petrology*, 62(2), ega107.
- Scoon, R. N., & Mitchell, A. A. (2012). The Upper Zone of the Bushveld Complex at Roossenekal, South Africa: geochemical stratigraphy and evidence of multiple episodes of magma replenishment. *South African Journal of Geology*, 115(4), 515-534.
- Sharma, J. J., Naik, A., Pant, N., Arora, D., Pandey, M., & Singh, P. (2021). Estimation of effective bulk composition—critical appraisal and a scanning electron microscope based approach. *Geological Journal*, 56(6), 2950-2962.
- Stüwe, K. (1997). Effective bulk composition changes due to cooling: a model predicting complexities in retrograde reaction textures. *Contributions to Mineralogy and Petrology*, 129(1), 43-52.
- Tegner, C., Cawthorn, R. G., & Kruger, F. J. (2006). Cyclicity in the Main and Upper Zones of the Bushveld Complex, South Africa: Crystallization from a Zoned Magma Sheet. *Journal of Petrology*, 47(11), 2257-2279.
- Thomas, C. (2020). 2529BB Roossenekal 1:50000. Council for Geoscience.
- Van Tongeren, J. A., & Mathez, E. A. (2013). Incoming magma composition and style of recharge below the Pyroxenite Marker, Eastern Bushveld Complex, South Africa. *Journal of Petrology*, 54(8), 1585-1605.

- Van Tongeren, J. A., Mathez, E. A., & Kelemen, P. B. (2010). A felsic end to Bushveld differentiation. *Journal of Petrology*, 51(9), 1891-1912.
- Van Tongeren, J. A., & Mathez, E. A. (2012). Large-scale liquid immiscibility at the top of the Bushveld Complex, South Africa. *Geology (Boulder)*, 40(6), 491-494.
- Von Gruenewaldt, G. (1971). Petrographical and mineralogical investigation of the rocks of the Bushveld Igneous complex in the Tauteshoogte-Roosenekal area of the Eastern Transvaal (Doctoral dissertation, University of Pretoria, Pretoria, South Africa).
- Von Gruenewaldt, G., Klemm, D. D., Henckel, J., & Dehm, R. M. (1985). Exsolution features in titanomagnetites from massive magnetite layers and their host rocks of the upper zone, eastern Bushveld Complex. *Economic Geology*, 80(4), 1049-1061.
- Wallmach, T., Hatton, C. J., & Droop, G. T. R. (1989). Extreme facies of contact metamorphism developed in calc-silicate xenoliths in the Eastern Bushveld Complex. *The Canadian Mineralogist*, 27, 509-523.
- Winter, J. D. (2013). Principles of Igneous and Metamorphic Petrology. –Pearson Education Limited.
- Yamasaki, T., & Uchino, T. (2023). Assimilation of lower-crustal dunite xenoliths into adakite-related felsic magma: New insights into the production of bajaitic high-Mg andesites. *Journal of Asian Earth Sciences*, 249, 105613.
- Yao, Z., Mungall, J. E., & Jenkins, M. C. (2021). The Rustenburg Layered Suite formed as a stack of mush with transient magma chambers. *Nature Communications*, 12(1), 505.
- Yuan, Q., Namur, O., Fischer, L. A., Roberts, R. J., Lü, X., & Charlier, B. (2017). Pulses of Plagioclase-laden Magmas and Stratigraphic Evolution in the Upper Zone of the Bushveld Complex, South Africa. *Journal of Petrology*, 58(8), 1619-1643.

APPENDIX

Table 5 - Description of thin sections including thin section scans in PPL

Sample number	Sample Description	Thin section scan
AA-21-01	<ul style="list-style-type: none"> • Host rock sample • Unaltered plagioclase with polysynthetic twinning • Opaque (magnetite) • Biotite + Muscovite • Small amount of interstitial Clinopyroxene 	
AA-21-06	<ul style="list-style-type: none"> • Altered euhedral plagioclase crystals, some of which have been sericitized • Large hornblende crystals • Strong pleochroism visible in amphibole from brown to blue/green. 	
AA-21-09	<ul style="list-style-type: none"> • Altered euhedral plagioclase crystals. • Actinolite and hornblende • Trellis exsolution of ilmenite found associated with green amphibole. 	

<p>AA-21-10</p>	<ul style="list-style-type: none"> • AA-21-10A: Large anhedral plagioclase with actinolite • AA-21-10B: • Euhedral plagioclase, largely unaltered • interstitial green amphibole and large hornblende crystals • small amounts of biotite • Partially altered magnetite, as well as unaltered magnetite and relict trellis ilmenite. 	
<p>AA-21-11B</p>	<ul style="list-style-type: none"> • Rim sample • Large altered euhedral plagioclase crystals • veins filled in with green amphibole, large hornblende crystals and interstitial green amphibole 	


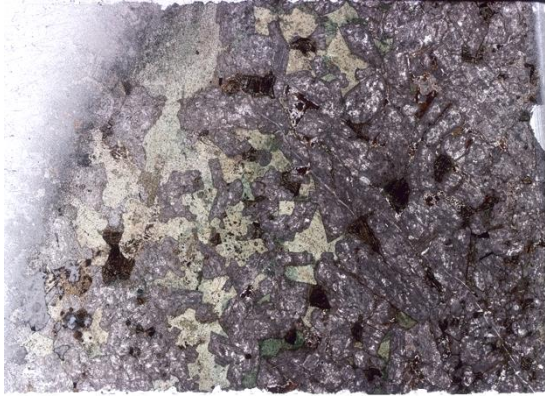











AA-21-11C	<ul style="list-style-type: none">• Core sample• euhedral altered plagioclase that is fractured and filled with green amphibole• interstitial green amphibole, large hornblende crystals	
AA-21-12	<ul style="list-style-type: none">• Altered euhedral plagioclase crystals• actinolite and hornblende.• Trellis exsolution of ilmenite found associated with green amphibole.• Sections of very fine grained, fibrous actinolite	

Table 6-Table showing all samples that were collected in the field along with a brief description and a photograph

Sample number	Sample Description	Field Photograph
AA-21-01	<ul style="list-style-type: none"> • Host rock sample taken on the northern bank of the river. • Sample is magnetic 	
AA-21-02	<ul style="list-style-type: none"> • Black/dark colour • irregular shape • is not magnetic • no reaction rim, but has a sharp contact with host rock 	
AA-21-03	<ul style="list-style-type: none"> • Layered appearance, • possibly silicic or metasedimentary • light grey colour with a darker central band <p>Sample A: Sample of lighter grey area</p> <p>Sample B: Sample of dark central band</p>	

<p>AA-21-04</p>	<ul style="list-style-type: none"> • Sharp contact with reaction rim • Core and rim areas • Core: Coarse grained euhedral plagioclase crystals in a dark matrix, • Rim: Fine grained, white colour, well defined. 	
<p>AA-21-05</p>	<ul style="list-style-type: none"> • Very large dark pegmatitic crystals of amphibole • Crystals are well defined and can be up to 2cm in length 	
<p>AA-21-06</p>	<ul style="list-style-type: none"> • Light grey gradual contact with darker well fined core • Core: Coarse grained plagioclase crystals in a dark matrix • Rim: finer grained and lighter in colour, large surrounding area 	
<p>AA-21-07</p>	<ul style="list-style-type: none"> • Black/dark colour • irregular shape • no reaction rim, but has a sharp contact with host rock 	

<p>AA-21-08</p>	<ul style="list-style-type: none"> • Black, Irregular shape • No reaction rim 	
<p>AA-21-09</p>	<ul style="list-style-type: none"> • Sharp contact with well-defined light coloured rim • Core: Coarse grained plagioclase crystals in a dark matrix • Rim: finer grained and lighter colour 	
<p>AA-21-10</p>	<ul style="list-style-type: none"> • +/- 60cm diameter, white matrix with anhedral black crystals. <p>Sample A: mostly white with large black crystals</p> <p>Sample B: mostly white with smaller finer grained black crystals</p> <p>Sample C: Mostly black crystals</p> <p>Sample D: Mostly white with anhedral interstitial black crystals</p>	

<p>AA-21-11</p>	<ul style="list-style-type: none"> • Very well-defined core and rim areas. • core: Coarse grained plagioclase crystals in a dark matrix. • rim: finer grained, pale colour, well defined <p>Sample A: taken in the rim</p> <p>Sample B: taken in the rim</p> <p>Sample C: taken in the core</p>	
<p>AA-21-12</p>	<ul style="list-style-type: none"> • Large euhedral plagioclase crystals with a dark interstitial mineral • +/- 1m diameter • Sharp contact, eroded on the edges • No reaction rim 	